



## **Abstract**

Several cores from the Eurasian Basin of the Arctic Ocean contain a distinct grey layer with several prominent features, including a sharp lower boundary and a lack of bioturbation, characteristic for a rapid deposition. Large amounts of ice-rafted debris is also found within the layer, suggesting high calving activity at the edge of the ice shelves. Lastly, the layer has low manganese content, pointing to oxygen-poor bottom and pore waters. It has been posited in previous studies that this layer was caused by a rapid drainage of an ice-dammed lake in northern Siberia during the Weichselian glaciation, between 50-60 ka. In this thesis, a number of methods were used to examine the grey layer, and ascertain if it was caused by the lake outburst. Visual inspection was used for initial identification, followed by the study of X-ray images and ITRAX-scans to choose suitable sampling depths. Isotope analysis of neodymium, samarium and strontium were subsequently performed to establish the source area of the sediment. Some cores contain several grey layers, or layers which do not match the 50-60 ka age, however these can be distinguished from the 50-60 ka layer using the methods described in this study. In layer occurrences which are chrono-stratigraphically consistent with the proposed lake outburst, the primary source of the sediment is identified as the Putorana plateau basalts and its weathering products. The findings presented here fully support the hypothesis that a rapid lake drainage from northern Siberia is the origin of the 50-60 ka grey layer.

## Table of Contents

1. Introduction	3
2. Aim of study	5
3. Background	6
4. Study area and core locations	29
5. Materials and methods	31
6. Results	35
7. Discussion	44
8. Conclusion	52
9. Acknowledgements	54
10. References	55

## 1. Introduction

The Arctic Ocean (AO) (Fig. 1.) consists of two major basins: the Eurasian Basin (which is the focus area for this study) and the Amerasian basin, separated by the Lomonosov ridge. The Gakkel spreading ridge, a continuation of the Mid-Atlantic ridge, divides the Eurasian basin into the Amundsen and Nansen basins. The Arctic Ocean is almost land-locked; the only deep water inlet is the Fram Strait.

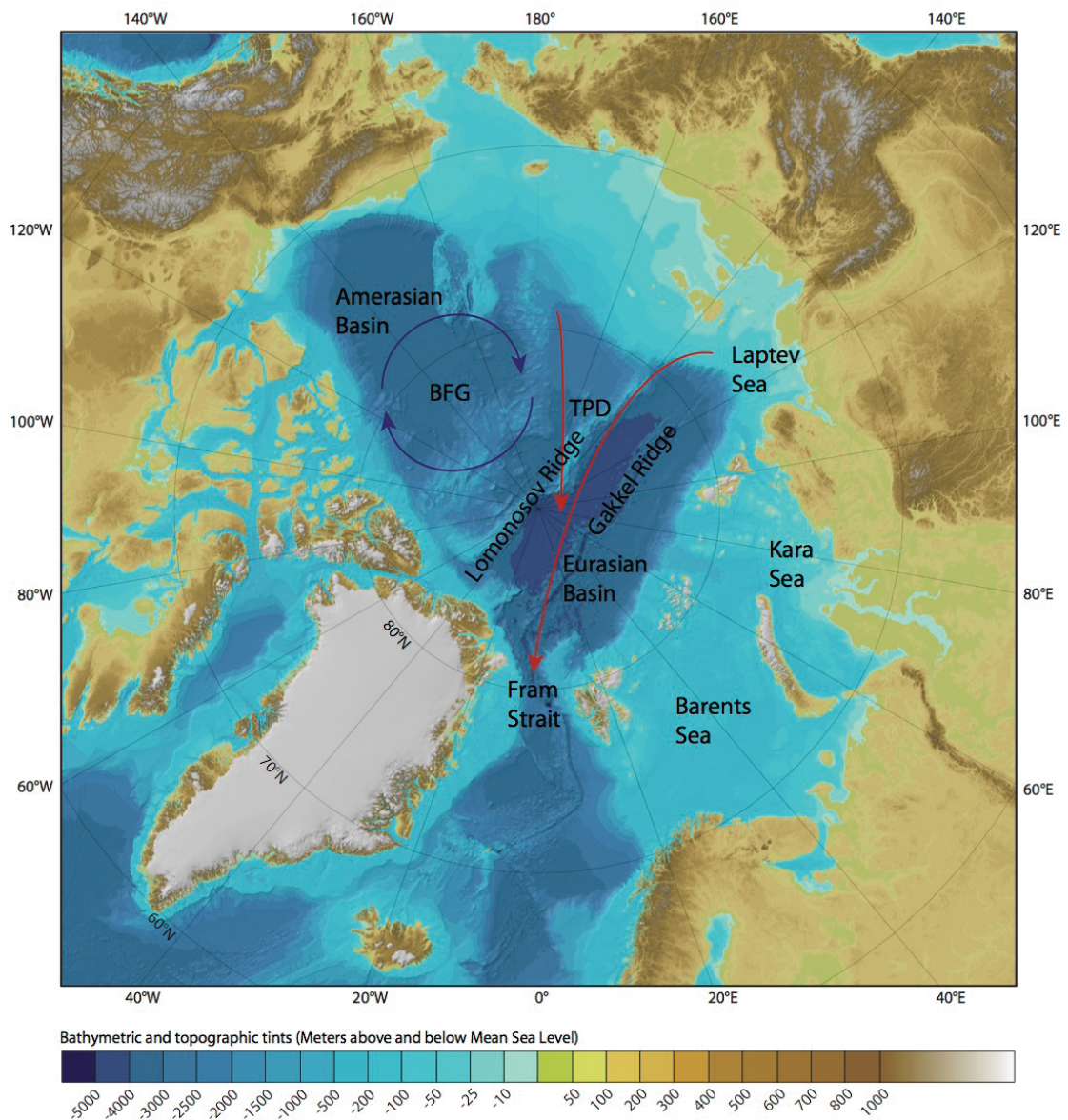


Fig. 1. The Arctic Ocean, with its two major currents: the Transpolar Drift (TPD) and the Beaufort Gyre (BFG). Modified from IBCAO (Jakobsson et al., 2012)

Several Russian rivers (including Ob, Yenisei, and Lena) drain into the Arctic Ocean. These rivers, along with ice formed at the continental shelves and coastlines in winter time, are responsible for carrying fine-grained sediment into the AO. During glacials, large inland ice sheets blocked the river drainage into the AO, leading to reduced sediment input (Fig. 2). The proportion of coarse grained material input is however increased, due to its entrainment in and transport by sea ice and ice bergs. Sea ice with large amounts of entrained sediment is often referred to as dirty ice. Icebergs may even transport very coarse grained material, referred to as ice-rafted debris (IRD). Once in the open ocean, these sediments are carried by the two major currents in the Arctic Ocean; the Beaufort Gyre and the Transpolar Drift (Fig. 1).

The Arctic Ocean continental shelves and coastline on the Eurasian side have been partially glaciated several times, with the last glacial maximum (LGM) attained approximately 20 ka BP (Mangerud et al., 2004) during the Late Weichselian. Two earlier Weichselian glacial maxima are identified by Svendsen et al. (2004); 60-50 ka for the Middle Weichselian and 100-80 ka for the Early Weichselian. Two major formation centres for the ice sheets are Scandinavia and the Barents-Kara Sea region, the latter supporting an ice sheet possibly covering the entire shelf (Landvik et al., 1998), although this is subject to debate (Svendsen et al., 2004). Ingólfsson and Landvik (2013) describe a largely ice-free Kara Sea during the Middle Weichselian. From the two formation centres in Scandinavia and the Barents-Kara Sea, the ice sheets spread east and south, respectively (Svendsen et al., 2004).

Although opinions vary on the exact extent of the ice sheet over northern Siberia (Landvik et al., 1998, Svendsen et al., 2004), which affected the flow of several Russian rivers (e.g. Ob, Yenisei) (Mangerud et al., 2004), this ice sheet did retreat after its Middle Weichselian maximum (Svendsen et al., 2004; Spielhagen et al., 2004; Lambeck et al., 2006). This retreat can possibly be linked to a large ice-dammed lake drainage by IRD, clay mineral and isotope analysis (Strand and Immonen, 2010, Immonen et al., 2014, this study).

A grey layer, observed in several sediment cores from the Eurasian basin, with a sharp lower boundary, coarser grains than the surrounding sediment and lows in both Mn content and bioturbation, was deposited at approximately 50 ky.

Through isotope analysis, supported by X-ray images and X-ray fluorescence data, aimed at pinpointing the origin of the grey layer, this study helps further the understanding of the role of ice dammed lakes and their rapid drainage. The rapid drainage of Lake Agassiz, at approximately 8.2 ka, affected global thermohaline circulation and thereby global climate (Barber et al., 1999; Teller et al., 2002), and the drainage of the proglacial Siberian lakes likely also influenced climate in a significant way (Mangerud et al., 2004; Krinner et al., 2004). Understanding these events is therefore an important factor in understanding climate change, both that of the last ice age, and the effect of melting ice today.

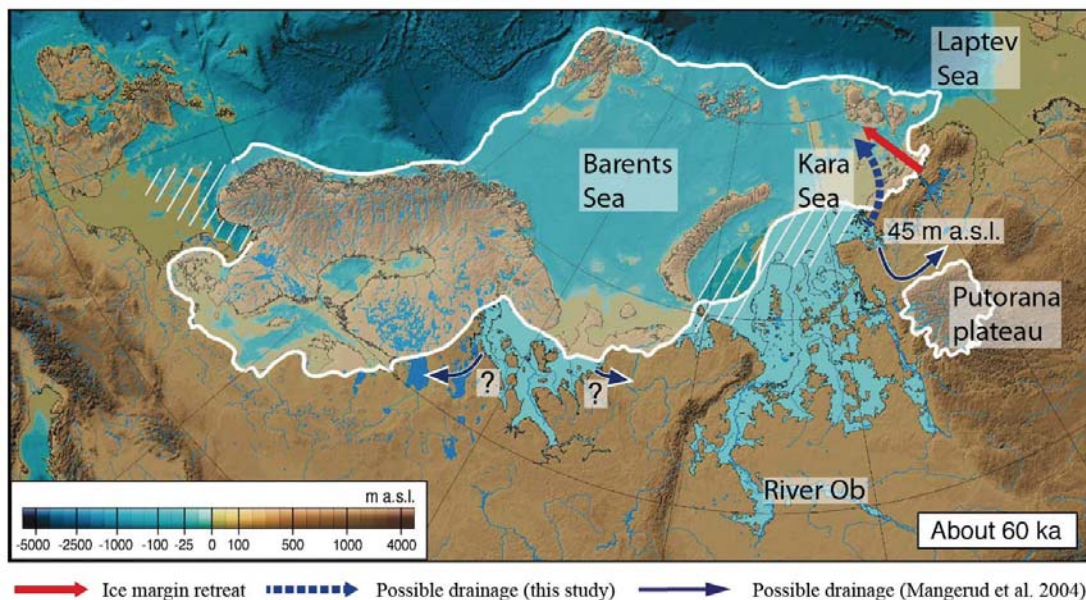


Fig. 2. The Weichselian ice sheet at approximately 60 ka. A large part of the Siberian hinterland is covered by an ice-dammed lake, formed by the blocked drainage of major north-flowing Russian rivers, including Ob and Yenisei. Two possible drainage routes of the lake are shown on the map: solid blue the one assumed by Mangerud et al. (2004), dashed inferred from sediment composition (this study). Modified from Mangerud et al. (2004).

## 2. Aim of study

The grey layer found in several Eurasian basin cores is the focus of this study. If this layer can be linked to the outburst of an ice-dammed lake, it has implications for the Weichselian glaciation, the climate of northern Russia at 50-60 ka, and Arctic Ocean conditions at the time. The points of inquiry are:

1. What are the identifying markers of the grey layer, and how does it differ from other grey layers?
2. Can the outburst of the ice-dammed lake be linked to the grey layer?
3. How would the outburst have affected bottom and pore water chemistry in the Arctic Ocean?

To pinpoint the origin of the grey layer, this study uses isotope measurements of neodymium (Nd), samarium (Sm) and strontium (Sr), which can be used to trace the source rock of sediment (e.g. Haley et al., 2008). These measurements are supported by X-ray images and ITRAX scans (performed and some previously used by Löwemark et al. (2008)).

### **3. Background**

#### **3.1 Arctic Ocean**

The two major basins of the Arctic Ocean are the Eurasian basin and the Amerasian basin. They are separated by the Lomonosov ridge, which stretches from Greenland to the Siberian shelf, across the North Pole. The Amerasian basin will not be described in detail as no cores used in this study were taken there. The Eurasian basin is in turn made up of the Nansen and Amundsen basins, separated by the Gakkel spreading ridge; an ultra-slow spreading continuation of the Mid-Atlantic ridge, which widens the Eurasian basin by 6-13 mm per year (Michael et al., 2001). The abyssal plain in the Eurasian basin reaches depths of over 4000 m, shallowing to 3200 m on the Gakkel ridge and 700 m on the Lomonosov ridge. In the southern part of the Eurasian basin, the Morris-Jessup rise extends from the Greenland shelf, and the Yermak plateau extends from the Svalbard shelf. The continental shelves are the broadest of any ocean, constituting over 50 % of the total Arctic Ocean sea floor area. The only deep inlet is through the Fram Strait, situated between Greenland and Svalbard (Jakobsson, 2002, 2003a).

The two major surface currents in the Arctic Ocean are the Beaufort Gyre, which flows clockwise in the Amerasian Basin, and the Transpolar Drift, which flows along the Lomonosov Ridge toward the Fram Strait (Fig. 1). These are

responsible for transporting sea ice and ice bergs, and also large quantities of sediment within dirty ice. Dirty ice forms in, among others, rivers, on coastal shelves and in fjords; anywhere where sediment can become entrained in ice. Coarse grained sediment transported in this way is often referred to as ice rafted debris (IRD). There are also several intermediate and deep water currents, but these are not capable of transporting coarse grained material (Sellén et al., 2010).

### **3.2 The Arctic Ocean as a sediment archive**

The Arctic Ocean holds an important climate record. The varying presence of ice-rafted debris in sediment is an indicator of the amount of sea ice and ice-bergs that has drifted through and melted in the Arctic, and fossils can be used both as productivity indicators and biostratigraphical chronology markers. As the Arctic is particularly responsive to global temperature change (sometimes referred to as polar amplification) (Lee, 2014), e.g cooling caused by the separation of Australia-Antarctica and the formation of the Antarctic Circumpolar Current (Moran et al., 2006) and warming by greenhouse gases (Stroeve et al., 2007), its sediments can be used to study both local and global changes.

Although the Arctic Ocean appears to have fairly consistent sedimentation rates of a few cm/ka (Backman et al., 2004), it is difficult to establish a chronostratigraphy as sediment cores taken contain few microfossils, and magnetic reversals are difficult to interpret (Jakobsson, 2003b). It has been suggested that the Amerasian basin has ultra-low sedimentation rates of mm/ka, but this is a misinterpretation which appears to have been caused by faulty age models, and realistic values are on the order of cm/ka (Backman et al., 2004). Cycles of varying Mn content and colour, and optically stimulated luminescence (OSL) dates, have been used in conjunction with magnetic reversals to establish working chronologies (Jakobsson, 2000, 2003b, Backman et al., 2004).

Comparisons of grain size (% weight of the >63 µm fraction) and bulk density show a strong correlation in Arctic Ocean piston and drill cores (O'Regan et al., 2008). O'Regan et al. (2008) used this in conjunction with magnetic

susceptibility and paleomagnetic inclination to link stratigraphic units in the ACEX cores (see section 3.2.1) and with nearby piston cores. The chronology based on Mn cyclicity and OSL dating used by Jakobsson et al. (2000) matches that of O'Regan et al. (2008). For an age model beyond MIS 6,  $\delta^{18}\text{O}$  variations were used to match drill and piston cores (O'Regan et al., 2008).

### 3.2.1 ACEX

The Arctic Coring Expedition (ACEX) in 2004 aimed at resolving some of the problems with Arctic Ocean chronologies. Previously, shorter piston cores, stretching back no further than 200-500 ka had been the basis for chronologies in the Arctic Ocean (Backman et al., 2004). During ACEX a 428 m long sediment record was recovered from four drill holes on the Lomonosov ridge (Fig. 3). O'Regan et al. (2008) used several proxies (paleomagnetic inclination, grain size, bulk density, magnetic susceptibility, radiocarbon dating and biostratigraphy ) on the ACEX record, along with two nearby piston cores, to establish a chronology beyond 200 ka. The oldest sediments recovered by the ACEX expedition were from the early Eocene/late Paleocene, before drilling into late Cretaceous age bedrock. The ACEX record shows a relatively ice-free Arctic with high productivity in the late Palaeocene; a greenhouse world. A first transition into an ice-house world occurred at 49 Ma, indicated by the presence of ice-rafted debris in the cores (Moran et al., 2006).

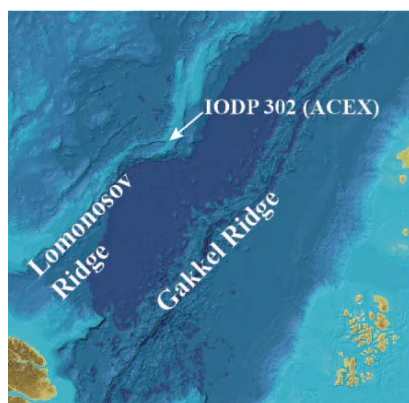


Fig. 3. Location of the coring sites during the ACEX expedition. Four sites were cored, between 87°52' and 87°56' N and 136° and 140° E.

### 3.2.2 Mn cycles

Arctic sediments often show a cyclicity in Mn content, which appears as alternating bands of brown (Mn-rich) and olive (Mn-starved) layers (Löwemark et al., 2008). The presence of Mn nodules in Arctic Ocean sediments indicate oxygenated bottom waters, because Mn is redox sensitive and precipitates as Mn oxide nodules in oxygenated waters, whereas nodules dissolve in oxygen-deprived waters (Yakushev and Newton, 2013). Jakobsson et al. (2000) used RGB-values of photos of a Lomonosov ridge-core, taken during the Arctic Ocean - 96 expedition (core 96/12-1PC), as a measurement for Mn content. The colour variations were correlated to oxygen isotope stages by taxonomic identification of nannofossils (e.g. *E. huxleyi* and *Gephyrocapsa* spp.) The flow of Mn from Siberian peat bogs was concluded as the main source for Mn variations, although this effect might have been reinforced by oxygenation variations. Löwemark et al. (2008) studied the same core using an X-ray fluorescence (XRF) scanner. The Mn values given by the XRF-scanner correlated with those of Jakobsson et al. (2000), with a few exceptions. Similar to Jakobsson et al. (2000), Löwemark et al. (2008) linked Mn variations to changes in input from Russian rivers and oxygenation. MacDonald and Gobeil (2011) attributed changes in Mn content to an altered redox cycle caused by sea level changes; lowered sea level would cause the normal seasonal Mn- and organic matter cycling on the shelf to be interrupted when shelves become exposed. Changes in riverine input – rivers are largely blocked during glacials – can be regarded as the main factor in Mn-glacial/interglacial cycles found in Arctic Ocean (Löwemark et al., 2014). This makes Mn colour cycles a useful tool for establishing chronologies. Mn transport from rivers to the marine basins of the Arctic Ocean occurs in multiple steps. Löwemark et al. (2014) describe Mn deposition occurring on the shelves, producing a temporary Mn sink. The Mn-oxides formed are however dissolved when seasonal biogeochemical activity depletes oxygen in bottom waters, leading to a cycling and step-wise transport from shelves into deep water. Deposition of Mn in the deep basins is linked to sea ice transport, both by the thawing of ice during summer and by bacterial/algal activity below the ice (Löwemark et al., 2014). The grey layer, which is the primary focus of this thesis, showed relatively high concentrations of Mn in the RGB data, but very low in the

XRF. In the top and bottom of the core, there were also differences between RGB and XRF data, the cause of which is unknown. Löwemark et al. (2008) also measured the variations in other elements. None matched the Mn variations, suggesting that the Mn input is decoupled from the input of terrestrial material, however the grey layer showed a distinct low in Fe and high in Ti.

The present study hypothesises that if the grey layer was rapidly deposited, it could explain the covariation in Fe and Mn, as they share a similar redox behaviour (e.g Lewis and Landing, 1991).

### **3.3 The Weichselian ice sheet and its ice dammed lakes**

The Eurasian ice sheet covered large parts of northern Europe during the Weichselian (110-10 ka). Ice sheets form on land, and the Weichselian ice sheet appears to have had one centre in northern Scandinavia, but also one in the Barents Sea (Siegert et al., 2002; Svendsen et al., 2004; Ingólfsson and Landvik, 2013). It grew in three main stages, with peaks in volume at approximately 90, 60 and 20 ka, the latest referred to as the last glacial maximum (LGM). At the 90 ka maximum, the ice covered most of Sweden and Norway, and extended across the Barents Sea shelf from Svalbard to the Putorana Plateau. The eastern extent of the 60 ka peak is somewhat uncertain, but similar to that of the 90 ka peak (Svendsen et al., 2004). To the west, it covered Scandinavia, the Baltic States and the Baltic Sea. By 20 ka, the ice covered Scandinavia, the Baltic States, northern Germany and Poland, and Great Britain, as well as Svalbard and the Barents-Kara continental shelves (Svendsen et al., 2005; Mangerud et al., 2004). Ice sheets transport sediment into marine environments by a number of mechanisms (Fig. 4). As ice sheets are deformed under their own weight, they flow slowly, eroding underlying rock and sediment, and depositing the eroded material as till, sometimes forming moraines. Additionally, meltwater rivers are formed under most ice sheets, and these deposit relatively coarse material in eskers. Sediment is also entrained in the ice as it moves toward the ocean. When the ice sheet reaches the ocean, it comes afloat and begins calving. When calved off icebergs melt, the entrained sediment is deposited on the sea floor (Siegert et al., 2002). The Barents-Kara ice sheet has left large deposits of glacial till and marks from

ice movement (furrows) on the Barents-Kara Sea continental shelves, including a large number of lineations and moraines in Svalbard fjords and on the shelves (Ottesen et al., 2007, Bjarnadóttir et al., 2013). Ice-rafted debris was also carried by the calving ice bergs and deposited in the deep basins (Siegert et al., 2002). The landforms left by the ice have been used by e.g. Ottesen et al. (2007) to map the waxing and waning of the Weichselian ice sheet. The outlets of large Russian rivers (including Ob and Yenisei) were blocked by the ice sheet, which stretched from Scandinavia along the Barents-Kara continental shelves to the Taimyr peninsula, leading to the formation of ice dammed lakes in the Siberian hinterland at both 90 and 60 ka (Mangerud et al., 2004). Evidence from sudden drainages of similar ice dammed lakes have been found e.g. in North America; Lake Agassiz (Fisher et al., 2002; Broecker, 2006), and Sweden; the final drainage of the Baltic ice lake (Björk, 1995; Jakobsson et al., 2007), and it is likely that such an event also occurred in Siberia. A catastrophic drainage of this kind, caused by the retreat of the eastern part of the ice sheet, was proposed by Mangerud et al. (2004) and would likely have carried with it large volumes of sediment from the lake and the area through which it flowed. Through erosion by the flow, but also possibly by an increased flow rate (Alley et al., 2008) where the flowing water acted as a lubricant, it would also have affected calving activity in the area, and possibly global ocean circulation (Mangerud et al., 2004). Spielhagen et al. (2004) found a large meltwater pulse at 50-60 ka, associated with the retreat of the Barents/Kara Sea ice sheet (Fig. 5). For further information on ice-dammed lake outbursts, see section 3.6.

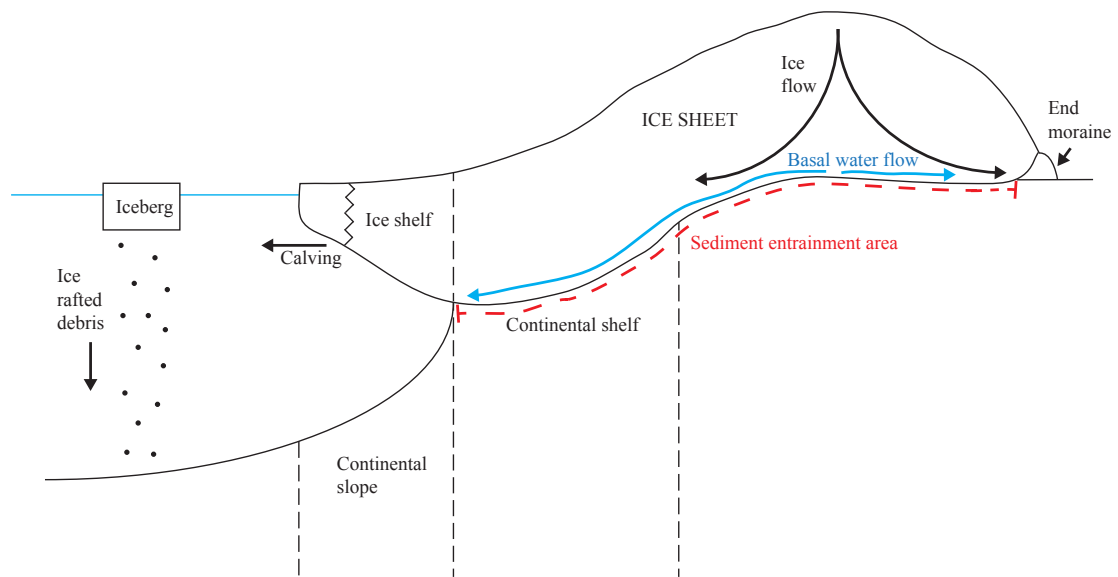


Fig. 4. Generalisation of the flow of ice and sediment entrainment and deposition by an ice sheet. Structures formed by basal water flow, such as eskers, are not included. End moraines may also form on the continental shelf.

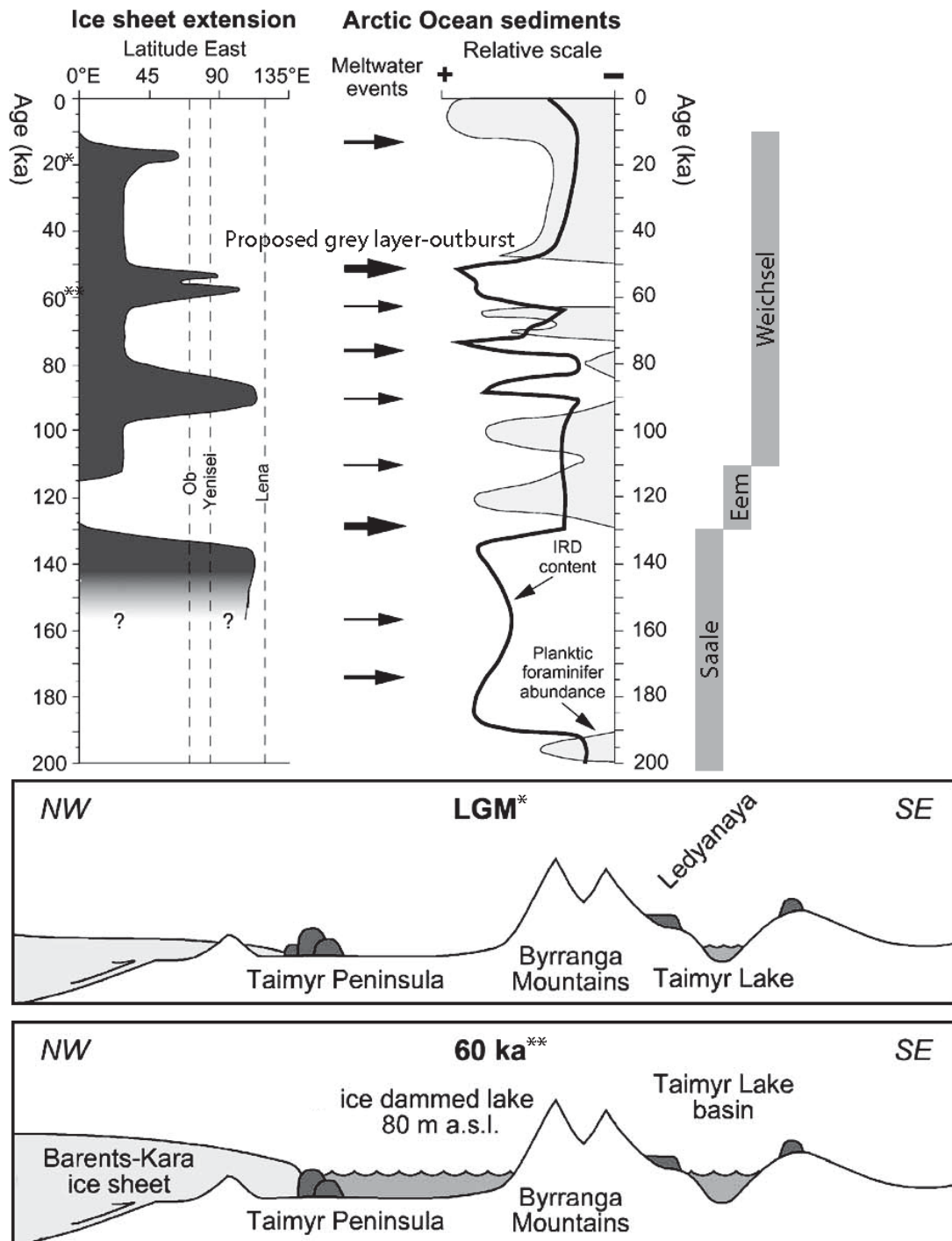


Fig. 5 (a) Maximum ice sheet extent at given age (left). Black arrows show meltwater pulses based on Spielhagen et al. (2004). The arrow size reflect relative meltwater volume. The retreat of the ice sheet between 60 and 50 ka is associated with the largest pulse in the Weichselian. (b) Cross-sections of the area between the Barents-Kara ice sheet and the Taimyr lake, showing the ice-dammed lake at 60 ka, and lack thereof at the LGM (20 ka). The Byrranga Mountains are located approximately 73-75°N and 90-110°E. Modified from Spielhagen et al. (2004) and Svendsen et al. (2004).

### 3.4 Present-day sediment sources to the Arctic Ocean

Sediment transport into the Arctic Ocean is controlled by river-input (including ice sheet basal melt water, enriched with sediments), entrainment of sediment in sea ice (producing dirty ice), and by ocean currents (mainly the Beaufort Gyre and Transpolar Drift). Sediment entrainment in sea ice occurs mainly on the flat continental shelves, and much on those of the Kara and Laptev Sea (Darby, 2003). Sediments are deposited there primarily during the spring floods (Nürnberg et al., 1994) and then frozen into the ice. Other, less important mechanisms for entraining sediment into the sea ice include river ice and discharge during other periods than spring (Nürnberg et al., 1994). Sea ice transports large amounts of sediment from the Russian shelves even into the Amerasian basin, where as much as 50 % of sea ice may be dirty ice (Nürnberg et al., 1994). Darby (2003) found that some 16% (or more in certain cases) Fe oxide grains in samples from northern Canadian shelves have Russian origins. Both Nürnberg (1994) and Darby (2003) cite the Laptev Sea as a major source of ice-entrained sediment, as evidenced both by the Fe oxide tracing by Darby (2003) and smectite measurements of ice samples from the central Arctic by Wahsner et al. 1999). The isotopic composition of sediment in modern sea ice in the Arctic Ocean matches the Kara and western Laptev Sea (Tütken et al., 2002). Wahsner et al. (1999) concluded that smectite can generally be used as a source area tracer for Arctic sediments, and is useful for transport pathways, although not for studying sea ice-transported sediment. The highest concentration of smectite in Arctic surface sediments can be found in the Kara and western Laptev Seas (Fig. 6), where it reaches >60 and 30-40 %, respectively (Nürnberg et al., 1995, Wahsner et al., (1999). Having only one major source area makes smectite particularly valuable proxy for sediment transport pathways (Vogt and Knies, 2008). Although sea ice in the central Arctic contains high amounts of smectite, originating in the Kara and west Laptev Seas (Tütken et al., 2002), clay minerals in central Arctic surface sediments are likely supplied as material suspended by ocean currents, and the ice-entrained sediment is deposited further south (Wahsner et. al, 1999; Winkler et al., 2002). Smectite in the Fram Strait is also likely not only from the Kara and Laptev Seas, as the distance allows mixing-in of material from other sources, such as Iceland (Winkler et al., 2002).

Smectite as a proxy for transport mechanisms in the Eurasian basin was also studied by Vogt and Knies (2008). Using box core samples (taken in an area approximately 90 °N to 80 °N by 30 °W to 40 °E), smectite content was measured and compared to carbon and oxygen isotope data to produce a time-line. It was found that highs in smectite could be tied to bursts of melt water and increased ice-berg production during the latest deglaciation. High concentrations of smectite could further be tied to peaks in organic matter content. Large fluctuations in smectite over the last 16 Ma can be found in cores from the Fram Strait, and is tied to variations in climate (Winkler et al., 2002). The sediment composition of the source areas can however be assumed to have varied little in the last 100 ka, as models (e.g. Mangerud et al., 2004) show similar river pathways as are present today.

Illite, found in its highest concentrations near Svalbard and in East Siberian Sea sediments, is the most prevalent clay mineral in surface sediments throughout the central Arctic. This would suggest that while the East Siberian Sea is not important for ice-entrained sediment (Darby, 2003), it might be a major contributor to clay-sized sediment transported by ocean currents.

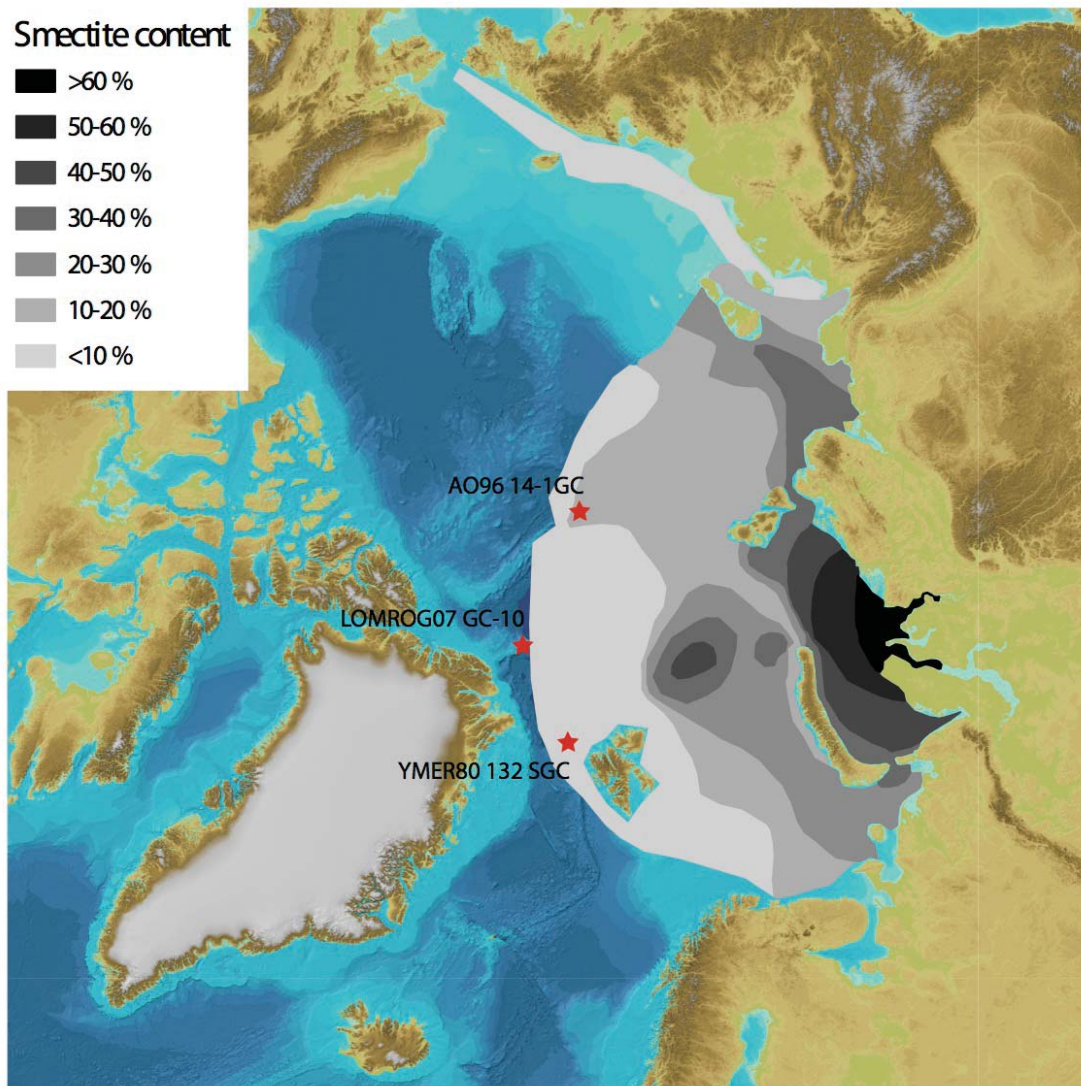


Fig. 6. Map of clay mineral distribution in the Eurasian Basin. Locations of cores investigated in this study indicated by red stars. Adapted from Wahsner et al. (1999).

### 3.5 The grey layer

A distinct grey layer has been found in the Eurasian Basin of the Arctic Ocean. The layer has the characteristics of a rapidly deposited layer: sharp lower boundary (Fig. 7 and 8) and heterogeneous geographical distribution (Fig. 9). The layer varies greatly in thickness, from 10-15 cm in LOMROG07 GC10 to 51 cm in AO96 12-1PC (Lövemark et al., 2008). It largely consists of IRD (Lövemark et al., 2008), and there is a complete lack of bioturbation. The clay mineralogy of the grey layer, with a distinct increase in smectite at the base, corresponds to the weathering components of the Putorana plateau and the Kara-Laptev shelf sediments, and has been preliminarily dated to the transition between Marine Isotope Stage (MIS) 3 and 4, 60-50 ka (Lövemark et al., 2009, Wahsner et al., 1999). It also contains a large amount of ice-rafted debris (IRD) and higher coarse fraction content than surrounding sediment, something that would be expected from a relatively high-energy event. Spielhagen et al. (2004) calculated accumulation rates 2-4 times above normal (an increase from 2.8 to 11.2 cm/ka based on sedimentation rates for MIS 5) for this layer, which they attribute to high calving activity of the Eurasian ice sheet caused by warm climatic conditions. In addition, they found distinct  $\delta^{18}\text{O}$ -peaks in foraminifera from the Fram strait, which they correlated to a large freshwater output from rivers and lakes in northern Russia. The possibility of a direct connection between these two events – i.e. increased calving caused by a catastrophic outburst of the ice dammed lake(s) – was however not made.



Fig. 7. X-ray photograph of grey layer lower boundary in core AO96 14-1GC. There is a distinct increase in IRD (white specks) and general grain size. Right is upward in the core. The boundary is at 166.5 cm core depth.

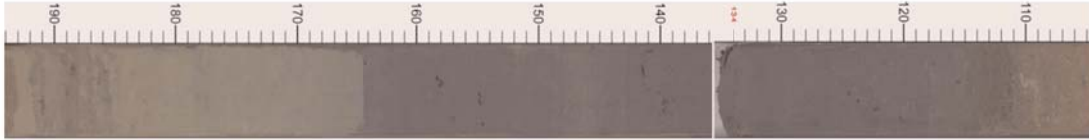


Fig. 8. Colour photograph of the grey layer in core A096 12-1PC. The layer begins at 164 cm and ends at approximately 113 cm depth in core. Modified from Jakobsson et al. (2000).

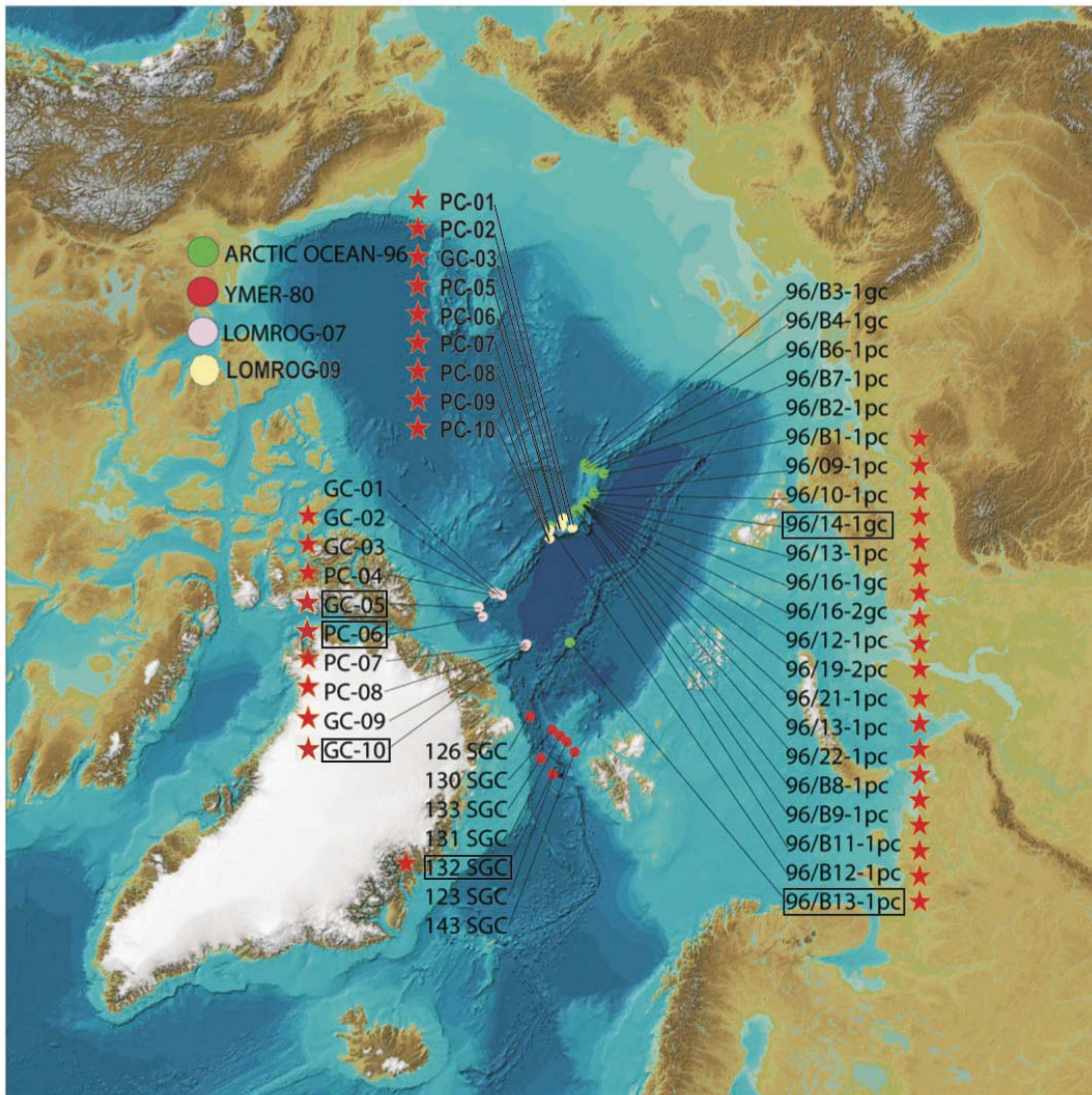


Fig. 9. All cores from the Ymer-80, Arctic Ocean -96, LOMROG -07 and -09 expeditions in which the grey layer has been observed. Modified from Mellquist (2009).

### 3.6 Ice-dammed lake outbursts

The connection between drainages of ice-dammed lakes and changes to global thermohaline circulation has been made in a number of studies (Barber et al., 1999; Teller et al., 2002). The latest deglaciation caused at least two major such drainages: lakes Agassiz/Ojibway (8400-8000 cal. yr BP, Barber et al., 1999) and the Baltic Ice Lake (11600-11700 cal. yr BP, Jakobsson et al., 2007). The volume drained from the former has been calculated to upwards of 163000 km<sup>3</sup>, with several drainages of 1600-9500 km<sup>3</sup> preceding it, (Teller et al., 2002), and the latter to 7800 km<sup>3</sup> (Jakobsson et al., 2007). For comparison, the volume of Lake Superior (the largest of the North American Great Lakes) is 12100 km<sup>3</sup> (<http://www.epa.gov/greatlakes/factsheet.html>). During the last deglaciation, at approximately 8.2 ky, there was a marked drop in global temperatures (1.5-3 °C in marine environments), resulting in a reversal of the deglaciation (Barber et al., 1999). This cold event can be linked to the last, and largest, drainage of lake Agassiz/Ojibway, which disrupted global thermohaline circulation (Barber et al., 1999; Teller et al., 2002). Mangerud et al. (2004) suggest that the build-up and subsequent drainage of a similar lake in the Siberian hinterland at ca 60-50 ky, could have had a similar effect on global climate. Models of the ice sheet suggest that the ice-dammed lakes had a regional cooling effect on climate surrounding the lakes, lowering temperature by as much as 10 °C (Krinner et al., 2004; Mangerud et al., 2004). The outburst of the lake in the Siberian hinterland would however have been far from North Atlantic Deep Water formation centres, making any effect on global climate unlikely.

### 3.7 Chemical background

#### 3.7.1 Neodymium, samarium and strontium

The isotopic composition of sediment can be used to trace its source area, and for this, neodymium (Nd), samarium (Sm) and strontium (Sr) are often used. Samarium and neodymium are lanthanides, with atomic numbers 60 and 62, and atomic weights of 144.242 and 150.36, respectively. Out of seven naturally occurring neodymium isotopes, the two used in this study are <sup>143</sup>Nd (stable) and <sup>144</sup>Nd (half-life of  $2.1 \times 10^{15}$  years,  $\alpha$ -decay). Samarium also has seven natural

isotopes, however only  $^{147}\text{Sm}$  is of any relevance to our subject matter, as it decays into  $^{143}\text{Nd}$  with a half-life of  $1.06 \times 10^{11}$  y ( $\alpha$ -decay). Strontium is an alkaline earth metal, with the atomic number 38 and atomic weight 87.62. In nature it is found as one of four stable isotopes; the ones of interest to this study being  $^{87}\text{Sr}$  and  $^{86}\text{Sr}$  (CRC Handbook of Chemistry and Physics, 2009).

Sm-Nd measurements have been used since the mid-1970s as a means of dating rocks of volcanic origin, although the very first attempts were conducted on meteorites (DePaolo and Wasserburg, 1976). As  $^{147}\text{Sm}$  decays into  $^{143}\text{Nd}$ , the initial  $^{143}/^{144}\text{Nd}$  ratio of the Earth can be calculated. McCulloch and Wasserburg (1978) observed that Sm/Nd-fractionation from the mantle values occurs when a part of the Earth's crust is formed, and this in turn affects concentrations. This fractionation occurs during fractional crystallisation.  $\text{Nd}^{3+}$  has a larger ionic radius than  $\text{Sm}^{3+}$  (Shannon, 1976), meaning it forms weaker bonds, and therefore it becomes enriched in the liquid phase. It was found by DePaolo and Wasserburg (1976) that patterns in rare earth elements in chondritic meteorites compared to Earth are similar (within 5 %), suggesting that Earth's mantle follows . The inference from this is that the mantle follows a Chondritic Uniform Reservoir (CHUR) evolution in the ratios of rare earths elements. Any deviation in  $^{143}/^{144}\text{Nd}$  from the CHUR in an igneous rock is measured in  $\epsilon\text{Nd}$ , which is calculated as follows:

$$\epsilon\text{Nd} = \left[ \frac{^{143}\text{Nd}/^{144}\text{Nd}_{\text{sample}}}{^{143}\text{Nd}/^{144}\text{Nd}_{\text{CHUR}}} \right] \times 10^4$$

The differentiation from CHUR that occurs can then be used to calculate the age of an igneous rock (DePaolo and Wasserburg, 1976; McCulloch and Wasserburg, 1978).

A fractionation of Sm/Nd in sedimentation processes does not occur (McCulloch and Wasserburg, 1978; Bros et al., 1992), and the age of the source rock of sediments can therefore be calculated.

### 3.7.2 Reservoir chemistry

This section will explain how Nd, Sm and Sr behave in the various reservoirs the sediment would have passed on its way to the Arctic Ocean sea floor (excluding source rock, which is detailed in section 3.7.1). It includes a section on iron (Fe) and manganese (Mn), because these elements form oxyhydroxides which Nd and Sm adsorb to. It will also describe the influence of the various properties of these reservoirs such as organic material and pH, on these elements.

#### *Fe and Mn*

Fe and Mn are two metals closely connected to Arctic Ocean sediments, as they form oxide/oxyhydroxide-nodules, similar in composition but smaller in size than those found in oxygenated waters e.g. in the Pacific. Rare earth elements (REE) are often incorporated in these nodules, and follow the redox cycles of Fe and Mn. This cycling is connected to oxygen content in the water, and a decrease often leads to dissolution of Fe/Mn-oxyhydroxides. Other factors that influence these compounds are the concentration of sulfur- and nitrogen compounds, dissolved organic matter and bacterial activity (Lewis and Landing, 1991). River transport, primarily by Russian rivers (MacDonald and Gobeil, 2012; Löwemark et al., 2014), is the major source for these elements in the Arctic Ocean.

Submarine volcanism (e.g. along the Gakkel ridge in the Arctic Ocean) can also contribute Fe and Mn to ocean waters (Middag et al., 2011). Under reducing conditions, which can be caused by high input of organic material or reduced ocean ventilation due to an extensive ice cover (Li et al, 1969; Löwemark et al., 2008, and section 3.2.2), Mn and Fe can diffuse through sediments until they reach oxidising conditions. In shelf areas with high productivity, especially during interglacial summers, the diffusion of Mn leads to a gradual transport of Mn from the shelves into deeper waters (Löwemark et al., 2014). In other areas with high Fe/Mn concentration in bottom waters, thick crusts or mats of nodules can be found, although this is not a feature found in the Arctic Ocean (Li et al, 1969). Fig. 10a is a generalisation of the speciation of Mn in a stratified water column. As the concentration of dissolved oxygen decreases, dissolved Mn begins to increase. Decrease in dissolved oxygen is usually caused by two factors: lack of mixing and oxidation of organic material. Bacterial activity does not only

scavenge dissolved oxygen, but also that from oxides present in the water column, e.g. Mn and Fe oxides (Yakushev and Newton, 2013).

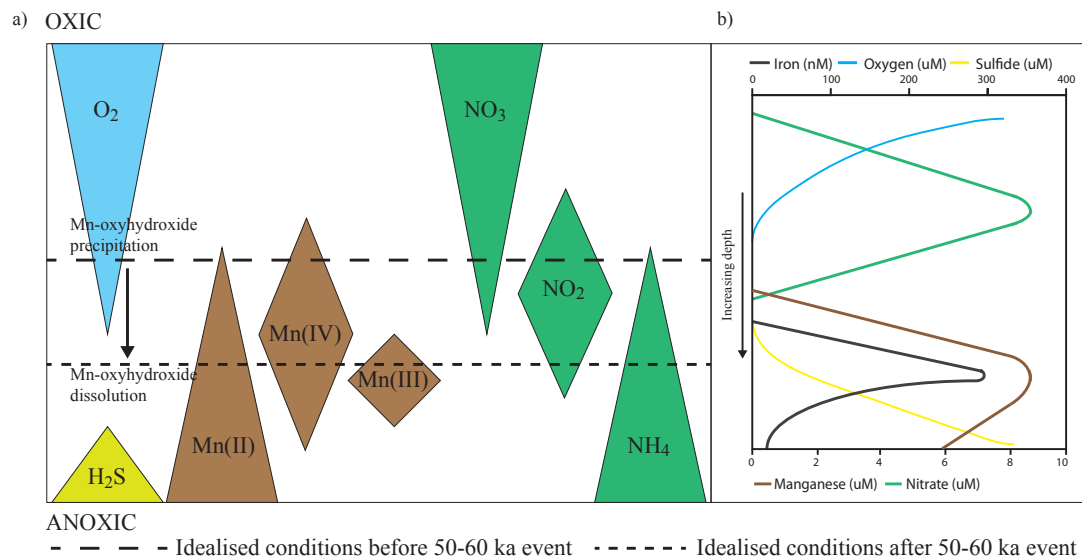


Fig. 10. a) shows the generalised speciation of manganese in a marine water column, in relation to dissolved oxygen, nitrogen-compounds and hydrogen sulfide. Adapted from Yakushev and Newton (2013). b) shows the concentration of dissolved iron, manganese, nitrate, oxygen and sulfide in relation to depth. The concentrations in this figure are for organic carbon rich waters (the Black Sea). Adapted from Lewis and Landing (1991).

Even if Arctic Ocean bottom waters were oxygenated at 60 ka, the deposition of the grey layer may have temporarily created reducing conditions in the sediment. The proposed ice-dammed lake was situated over what today is an area with many peat bogs, suggesting high amounts of organic matter may have been transported by the outburst. Löwemark et al. (2014) noted the presence of organic matter as a key component in the dissolution of Mn, and the resulting diffusion through sediment. If large amounts of organic matter was deposited by the lake outburst, the breakdown of this would cause oxygen depletion in the pore waters, and the thick grey layer would act as a lid, preventing any oxygen in bottom waters from rapidly counteracting oxygen depletion in pore waters.

The redox cycling of Fe and Mn has been studied extensively in the Black Sea (e.g. Lewis and Landing, 1991, German et al., 1991, Wijsman et al., 2001), and although there are several dissimilarities between the Black Sea and the Arctic

Ocean, the anoxic conditions present in the former could provide useful insight into the conditions after grey layer deposition. The depth of the redox interfaces in the Black Sea lie at between 70-110 m for Mn and 85-160 m for Fe (Lewis and Landing, 1991). Figure 10b shows simplified Fe/Mn redox interfaces in the Black Sea, adapted from Lewis and Landing (1991). Oxygen decreases rapidly with depth, reaching near depletion at 10-40 m (German et al., 1991). At the same approximate depth, nitrate concentrations peak before sharply decreasing. Dissolved Mn increases near the deeper nitrate minima. Fe increases sharply in concert with a slow sulfide increase. Both Mn and Fe show peaks at low sulfide concentrations, but higher concentrations leads to the formation of Fe/Mn-sulfides and subsequent decrease in dissolved Fe/Mn (Lewis and Landing, 1991; Pakhomova and Yakushev, 2013). German et al. (1991) present a clear connection between dissolved Mn and dissolved rare earth elements in the Black Sea. The elements Ce, Nd and Er display peak (180, 80, and 15 pmol/kg respectively) dissolved concentrations 100-400 m below the Fe/Mn redox interfaces, and very low (5-25 pmol/kg) concentrations above the interfaces (German et al., 1991).

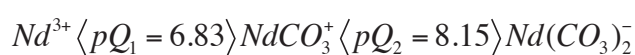
Mn input into the Arctic Ocean can primarily be attributed to coastal erosion and riverine input, although hydrothermal activity, e.g. along the Gakkel ridge, constitutes a smaller source (MacDonald and Gobeil, 2011; Middag et al., 2011). During interglacials, dissolved Mn shows a negative correlation with salinity (suggesting transport by river water) and is found in its highest concentrations along the shelves (Middag et al., 2011). Dissolved organic carbon shows a similar negative correlation with salinity (Wheeler et al., 1997). During glacials, the rivers would be blocked by large ice sheets on the shelves, causing lower concentrations of Mn in deep basins, and transport from the shelves limited to ice-rafting of Mn oxides (Middag et al., 2011). By extrapolating from deep basin conditions, Middag et al. (2011) suggested that large amounts of Mn are removed in shelf areas. MacDonald and Gobeil (2011) however considered this unlikely, as the high organic carbon on the shelves would cause oxygen-depleted conditions and prevent Mn oxide precipitation. Instead they proposed instead diffusion transport of Mn from shelves to deep ocean during interglacial summers, with precipitation of Mn oxides beginning on the shelf edges.

Interglacial winters instead would have suspension freezing as a primary Mn transport mechanism. Glacial conditions would see little dissolved Mn transport to the deep basins, with much of it stored in permafrost or shelf areas. Some entrainment of Mn oxides in ice, along with turbidite transport at the shelf edges, would occur (MacDonald and Gobeil, 2011).

## Neodymium

The main source of Nd in the world's oceans, rivers and lakes, is weathered continental crust, excluding carbonate-rich sediments and sedimentary rocks which have a low Nd content, with only a small input from hydrothermal sources (Palmer and Elderfield, 1986). The average abundance of Nd in sea water is  $2.8 \times 10^{-6}$  ppm (CRC Handbook of Chemistry and Physics, 2009), with local variations depending on riverine input and weathering. Global processes do not affect Nd to a great extent, as its residence time is less than the mixing time of the oceans (Palmer and Elderfield, 1986).

In sea water, Nd usually exists as free ions or carbonate complexes, depending on pH (see also Fig. 11):



(Byrne, 2002),

where  $pQ_1$  and  $pQ_2$  are the equilibrium constants between the species.

The speciation of REEs is also sensitive to the amount of dissolved organic matter, forming complexes with e.g. humic acids (Tang and Johannesson, 2003, Tanizaki et al., 1992) (see Fig. 11). As Nd (and Sm) in sea water appear dominated by carbonate complexes, complexation with organic matter likely occurs mainly in rivers, lakes, and possibly in pore water. Some ocean basins with a high concentration of dissolved organic matter, such as the Black Sea, may see more Nd/Sm-humic acid complexation.

Further, studies on river water (Tanizaki et al., 1992; Dupré, 1999; Tang and Johannesson, 2003) have shown that  $\text{Fe}^{3+}$  and  $\text{Al}^{3+}$  behave in a similar way to REEs, complexing with dissolved organic matter. Tang and Johannesson (2003) demonstrate that up to 11% of REE-organic complexes are replaced by Fe/Al-organic complexes if  $\text{Fe}^{3+}/\text{Al}^{3+}$  is present in a solution.

Neodymium in pore water is closely connected to Fe-Mn-oxyhydroxides, forming complexes or adsorbing to these (Tang and Johannesson, 2003). Any process which dissolves Fe-Mn-oxyhydroxides will also lead to mobilisation of Nd. In a

system where no such dissolution occurs, the adsorption of Nd is increased with increasing pH (Posselt et al., 1968). Murray (1974) performed a study where synthetic Mn oxides surface charges were measured in a solution with step-wise increased pH (pH 2 to 11). As the oxides exhibited an increasingly negative charge as pH was increased, higher cation adsorption may be at least partially attributed to this. In areas with high deposition of organic matter, Nd in pore water is likely to form complexes with organic matter as well. Neodymium in detrital material is not fractionated by sedimentation (McCulloch and Wasserburg, 1978; Bros et al., 1992). Neither does neodymium ratios seem affected by any grain size variations in sediment (Eisenhauser et al., 1999), i.e. no fractionation occurs during weathering of source rock. Haley et al. (2008) show that [authigenic] metal oxide coatings of Arctic sediments are sea-water derived.

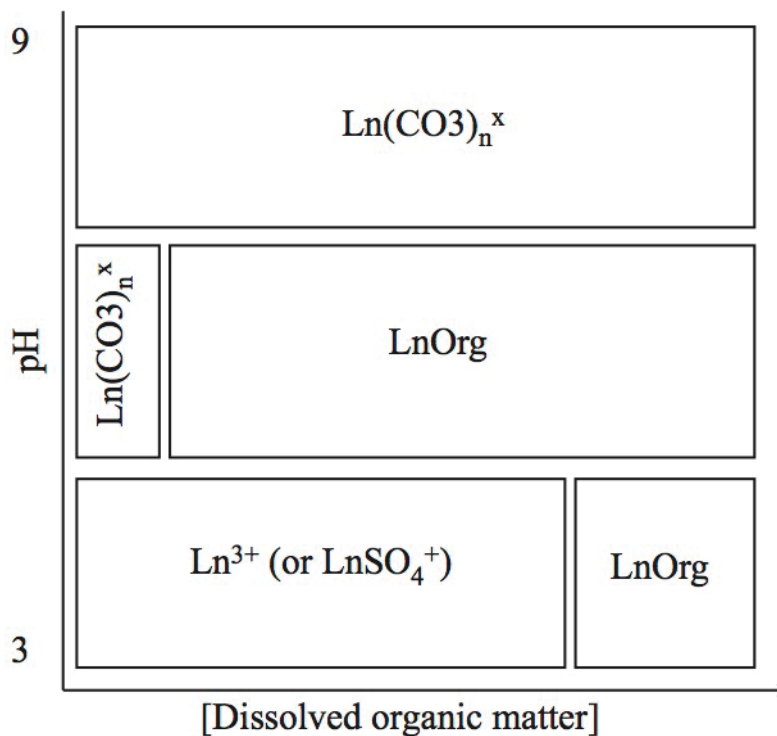


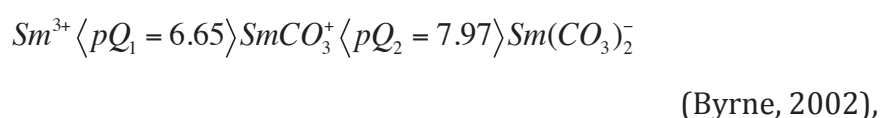
Fig 11. Generalised diagram of REE speciation depending on pH and concentration of dissolved organic matter. Ln is a placeholder for a lanthanide ion with a 3+ charge. Note that box borders are not absolute values as this is a summary of both text and diagrams. Adapted from Tang and Johannesson (2003).

Neodymium enters the Arctic Ocean through a number of transport pathways. The Russian rivers Kolyma, Lena, Yenisei and Ob, along with Atlantic water

through the Fram strait, are major Nd contributors to the Eurasian basin, while the Amerasian basin receives Nd input from the Mackenzie river and the Bering Strait (Porcelli et al., 2009). These various sources have widely differing isotopic signatures, e.g. the Lena river has a  $\epsilon\text{Nd}$  value of -14, while the Yenisei river has a value of -5 (Zimmerman et al., 2009). This allows for the use of Nd as a water mass tracer. Porcelli et al. (2009) observed distinct differences in Nd behaviour in river estuaries when comparing the Mackenzie river in Canada to Siberian rivers. This difference, a decrease in Nd concentrations in the transition from river to shelf water, is attributed to complexation with humic acids and Fe. Studies of leachates of Arctic Sediments have shown that the neodymium signature of bottom waters is recorded in authigenic sediment particles (Haley et al., 2008), with no significant difference in  $\epsilon\text{Nd}$  values between core top samples and present day sea water. These authigenic particles can therefore be used as a record of changes in Arctic Ocean deep/bottom water chemistry.

### *Samarium*

The chemical characteristics, origin and behaviour of samarium is similar to that of neodymium. Its concentration in sea water is lower ( $4.5 \times 10^{-7}$  ppm) (CRC Handbook of Chemistry and Physics, 2009), but exists in the same species as neodymium does:



where  $pQ_1$  and  $pQ_2$  are the equilibrium constants between the species.

Because the chemical characteristics of samarium are similar to those of neodymium, e.g. almost identical complexation in sea water (Byrne, 2002), it is assumed that its adsorption behaviour is also similar. As samarium has a smaller ionic radius than neodymium (Shannon, 1976), it is possible that it adsorbs more strongly. Samarium in detrital material is not fractionated by sedimentation (McCulloch and Wasserburg, 1978; Bros et al., 1992).

### *Strontium*

The concentration of strontium in sea water is 7.9 ppm (CRC Handbook of Chemistry and Physics, 2009), existing either as  $\text{Sr}^{2+}$  (86%) or as undissolved  $\text{SrSO}_4$  (14%), and does not appear to be prone to complexation (Byrne, 2002).

Studies by Posselt et al. (1968) and Murray (1974 and 1975) all show that Sr adsorbs, with increasing strength at increasing pH, to Mn oxides. Grain size is a factor in Sr measurements, as fine grained sediments, at least in the Arctic Ocean, appear to have a higher  $^{87/86}\text{Sr}$  ratio than coarse grained sediments (Tütken et al., 2002).

### *Organic carbon*

Organic carbon content in surface sediments varies between 0.5 and 2 % in the Eurasian part of the Arctic Ocean where the highest values are found in the Nansen Basin and north of Svalbard (Stein et al., 1994). Terrigenous input appears to be the major contributor of organic carbon, and the Siberian shelf is noted by Stein et al. (1994) as the primary source area, with silt stones and coal found as IRD. The increased calving activity following the lake outburst proposed by Mangerud et al. (2004) can be assumed to have increased the transport of organic carbon in this form to the Eurasian Basin.

## **4. Study area and core locations**

### **4.1 Sample locations**

The cores mentioned in this study were retrieved from the Eurasian basin of the Arctic Ocean, and from the Lomonosov Ridge. The wide geographical distribution was chosen to ensure that local changes would not be misinterpreted as basin wide events. AO96 14-1GC was taken on the Lomonosov Ridge close to the North Pole, and LOMROG07 GC-05 and PC-06 were taken further south on the ridge. LOMROG07 GC-10 was taken on the Morris-Jessup Rise north of Greenland, and YMERO80 132 SGC on the Yermak Plateau, on the opposite side of the Fram Strait. AO96 B13-1PC was taken on the Gakkel Ridge. (Fig. 9)

### **4.2 Putorana plateau**

The Putorana plateau (approximately 67-75 °N by 85-100 °E) is a >1000 m high basalt plateau and the most prominent part of the Siberian traps, the largest continental flood basalt province on Earth (Saunders and Reichow, 2009). It has a distinct isotopic signature (Fig. 12) in the rare earth elements (REE) samarium (Sm) and neodymium (Nd) (Sharma et al., 1992), which translates to the sediments formed by its weathering (Palmer and Elderfield, 1986). Weathering of the Putorana basalts also produce large amounts of smectite, heavily influencing the clay mineralogy of the Kara Sea, and to some extent also the Laptev Sea (Fig. 6) (Wahsner et al., 1999). The eastern edge of the Eurasian ice sheet probably reached the Putorana plateau at about 60 ka (Fig. 13) (Mangerud et al., 2004).

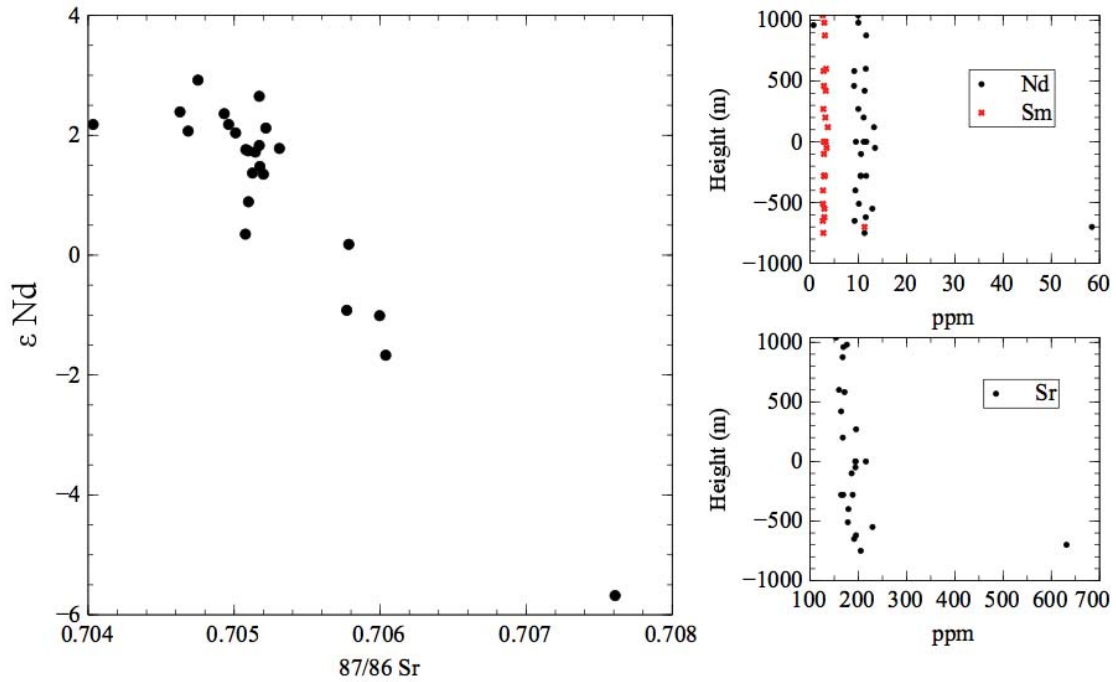


Fig. 12. Isotopic composition and element concentrations in Putorana rock samples ( $\epsilon_{Nd}$  to  $^{87}/^{86}Sr$  ratio [a] and concentration of Nd, Sm [b] and Sr [c]). Data from Sharma et al. (1992).

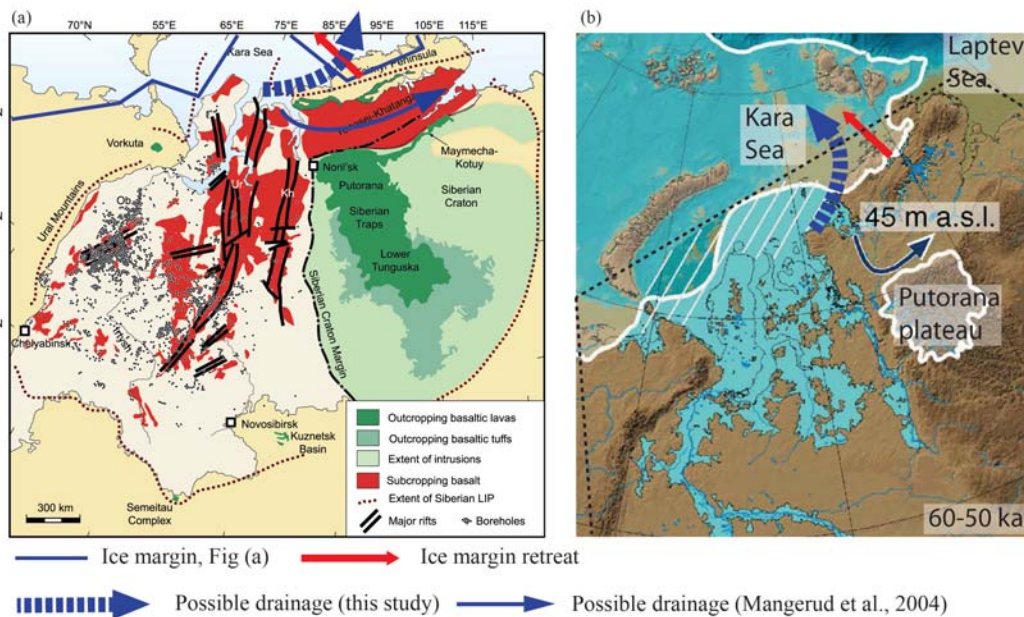


Fig. 13. (a) shows two proposed drainage routes of the 50-60 ka ice-dammed lake imposed on a geologic map of the Putorana basalts (modified from Saunders and Reichow, 2009). (b) shows the same on a topographical map with a paleogeographic reconstruction of the exposed shelves and ice dammed lake at 50-60 ka (modified from Mangerud et al., 2004). Ice margin on (b) is represented by the white solid line. Hatched area represents uncertainties in ice sheet extent. Black dashed line represents approximate of a) if overlain on b).

## 5. Materials and methods

### 5.1 Core selection

Due to time and budget constraints, this study was limited to three cores, obtained during the Ymer -80, Arctic Ocean -96 and LOMROG -07 cruises (Fig. 9). These were chosen to ensure a wide geographical distribution, and showed the presence of a grey layer at a depth which could reasonably correspond to 50ky, based on published age models for nearby cores (e.g. Löwemark et al. 2014) and previously calculated sedimentation rates of 1-5 cm/ka (e.g. Jakobsson et al., 2000; Backman et al., 2004). Core AO96 14-1GC was used in the pilot study, and was sampled at six locations; two samples above, two samples in (marked \*) and two samples below the grey layer. The cores LOMROG07 GC10 and YMER80 132 SGC were only sampled below and in the grey layer, due to budget constraints. Several other cores with reported grey layer, and of which there existed ITRAX-scans and/or X-ray images, were also visually inspected (Table 1).

Core	Location of grey layer (cm core depth)	Sampled depths (cm core depth)
AO96 14-1GC	167 – 149 cm	140, 150, 160*, 164*, 170, 180
AO96/B13 1PC	4 grey layers	-
LOMROG07 GC-05	142 – ?**	-
LOMROG07 PC-06	157 – ?**	-
LOMROG07 GC-10	49 – ca 35 cm	40*, 48*, 51, 60
YMER80 132 SGC	144 – 128 cm	140*, 143*, 145, 150

Table 1. Sampled cores, depth of grey layer in cores and sample depths. Samples taken within grey layer marked \*. Grey layers marked \*\* had a highly indistinct upper boundary.

#### 5.1.1 Identification of sampling depth in cores

The preliminary distinction of grey layers of the correct approximate age was based on the depth of the grey layer in the core. Based on a sedimentation rate of 1-5 cm/ka (see section 5.1), the depth interval 50-250 cm was investigated for a 50-60 ka layer, based on sediment colour and grain size. The grey layer is indicated by an abrupt change from olive-green-brown to grey colour, coupled with a coarser texture of the sediment (Löwemark et al., 2008, describe the layer

as mostly comprised of IRD). When possible, comparison was then made with X-ray pictures and XRF-data from previous studies (Mellquist, 2009). For further details on X-ray and XRF data, see sections 5.2.1 and 5.2.2. The use of X-ray pictures was intended to help identify large IRD concentrations, while the XRF data was used to track conspicuous variations in element concentrations, especially a Mn minimum within the entire grey layer, as reported by Löwemark et al. (2008). The methods for selecting sampling depths were not flawless, as is discussed in section 7.6.

## 5.2. Sample preparations and analytical methods

### 5.2.1 X-ray imaging

X-ray images of the cores are excellent non-destructive tools to further help visual examination. Using these, it is possible to better identify layers with coarser material, which is associated with the lower boundary of the grey layer. X-ray images were taken by Ludvig Löwemark at the Alfred Wegener Institute for Polar and Marine Research. Sampling was done by pressing down an approximately 10x6x0.5 cm plastic box into one half of the core. This was then cut out using nylon string, the box put in a plastic bag, the air sucked out, and the bag sealed. This plastic box can be X-rayed as is, meaning the sample can be reused. The sampling method is vulnerable to particularly loose sediments, and sometimes air bubbles can be created during the sampling process. Larger pieces of rock (>1 cm) must be removed before sampling.

### 5.2.2 XRF measurements

An XRF scan is a non-destructive way of measuring element composition in a core. It works by transmitting X-ray radiation onto a sample, and the fluorescence emitted by the different elements in the sample is then measured. However, the X-ray fluorescence also varies depending on e.g. the water content and material of the sample. The accuracy of these measurements also varies between elements, but Fe and Mn can be accurately measured. The instrument used on the samples in this study is the ITRAX XRF scanner at Stockholm

University. For more details on the scanner and methods used, see Löwemark et al. (2008) and references therein.

### 5.2.3 Carbon and nitrogen content and isotopic composition

Samples for carbon and nitrogen content and isotopic composition analysis were taken at regular (approx. 10 cm) intervals in the cores, with additional samples close to and in the grey layer(s), and weighed. They were then freeze dried for 3 days, weighed again in order to calculate water content and ground in an agate mortar. For the first measurement of organic matter content, the samples were heated to 105, 550 and 950 °C, and weighed between heatings. For the second measurement, approximately 5 mg of sample was placed in a silver capsule, and HCL (1M) added to dissolve carbonates. Carbon and nitrogen concentration and isotope analysis was then performed using a Finnigan DeltaV advantage connected to a CarloErba NC2500 at the Stable Isotope Laboratory, Department of Geological Sciences, Stockholm University.

### 5.2.4 Radiogenic isotope measurements

Samples for radiogenic isotope measurements were taken only close to and in the grey layer, due to higher analysis cost. They were then freeze dried for 3 days and ground using an agate mortar.

An initial bulk analysis was performed using the dissolution and ion exchange process described below. The results however prompted separation of terrigenous and authigenic material. This is explained further in section 6.4.2.

In order to separate the sea-water signal from the terrigenous signal, authigenic Fe/Mn micronodules (which precipitate from sea-water) had to be removed from the detrital material and therefore the sample was leached. This was done by weighing in approximately 0.12 g sample in a 50 ml conical centrifuge tube, adding 10 ml of a 1-1 mix of 25% acetic acid and 1M hydroxylamine hydrochloride and immersed in 90°C water for 3 hours. The tube was then centrifuged and the leachate decanted. The remaining detrital material was

rinsed with 10 ml UP H<sub>2</sub>O, centrifuged and decanted an additional 2 times, adding these 20 ml to the first 10 ml of leachate. This procedure ensured that no leaching solution remained with the detrital material, and the large amount of leachate produced allowed for 10-15 repetitions of the following ion-exchange; a safe-guard against spills and contamination.

Approximately 2 ml leachate was then spiked for Nd and Sm, evaporated to dryness and dissolved in 5 ml 4M HCl, making it ready for the ion exchange. The detrital material was dried in an oven at 60°C, and then dissolved in a mix of 2 ml conc. HF and 20 drops of conc. HNO<sub>3</sub> in a Teflon vessel. This was put in an oven at 200 °C for 3 days, and then taken out and evaporated to dryness. The samples were then dissolved in conc. HNO<sub>3</sub> and evaporated to dryness 3-5 times to remove any fluorides. They were then dissolved again in conc. HCl, and put in an oven at 200 °C overnight. After this, they were again evaporated to dryness and dissolved in 5 ml 4M HCl. This solution was then spiked for Nd and Sm.

For both leached and detrital material, the same ion exchange procedure was used. Nd, Sm and Sr were separated and extracted in ion exchange column, according to a method developed by Hans Schöberg at the Museum of Natural History, Stockholm, in part based on the work of Gutjahr et al. (2007).

For a detailed description of the ion exchange, see appendix 1.

## **6. Results**

This section presents a visual description of the cores and the results from radiogenic isotope analysis. It also presents X-ray pictures and XRF-measurements, courtesy of Ludvig Löwemark.

### **6.1 Visual examination**

All cores were visually similar at the transition into the grey layer. In all cores where it was found, the grey layer showed a sharp lower boundary, with a colour change from olive-brown-green to grey sediment. In A096/B13 1PC, four grey layers, all thinner than in the other cores, were found. As this core was not sampled, it is uncertain whether any of these layers corresponds to the 50-60 ka event, or are the results of smaller events. In several cores, the upper boundary was indistinct; a gradual transition from grey back to olive-green-brown (Fig. 8).

### **6.2 X-ray images**

Analysis of the X-ray images showed a sharp increase in coarse material at the lower grey layer boundary, and a gradual transition back to finer grained sediment upwards (Fig. 14a). Below and above the grey layer, there are clear marks of bioturbation, however it is completely absent in the grey layer (Fig. 14b). Notable features in the X-ray images are several X-mm sized grains (IRD), traces of bioturbation above and below the grey layer (visible as darker tracks), voids (much darker than the sediment), harder layers (likely large concentrations of authigenic particles or sand lenses) and skewed layers (usually caused by deformation during core retrieval).

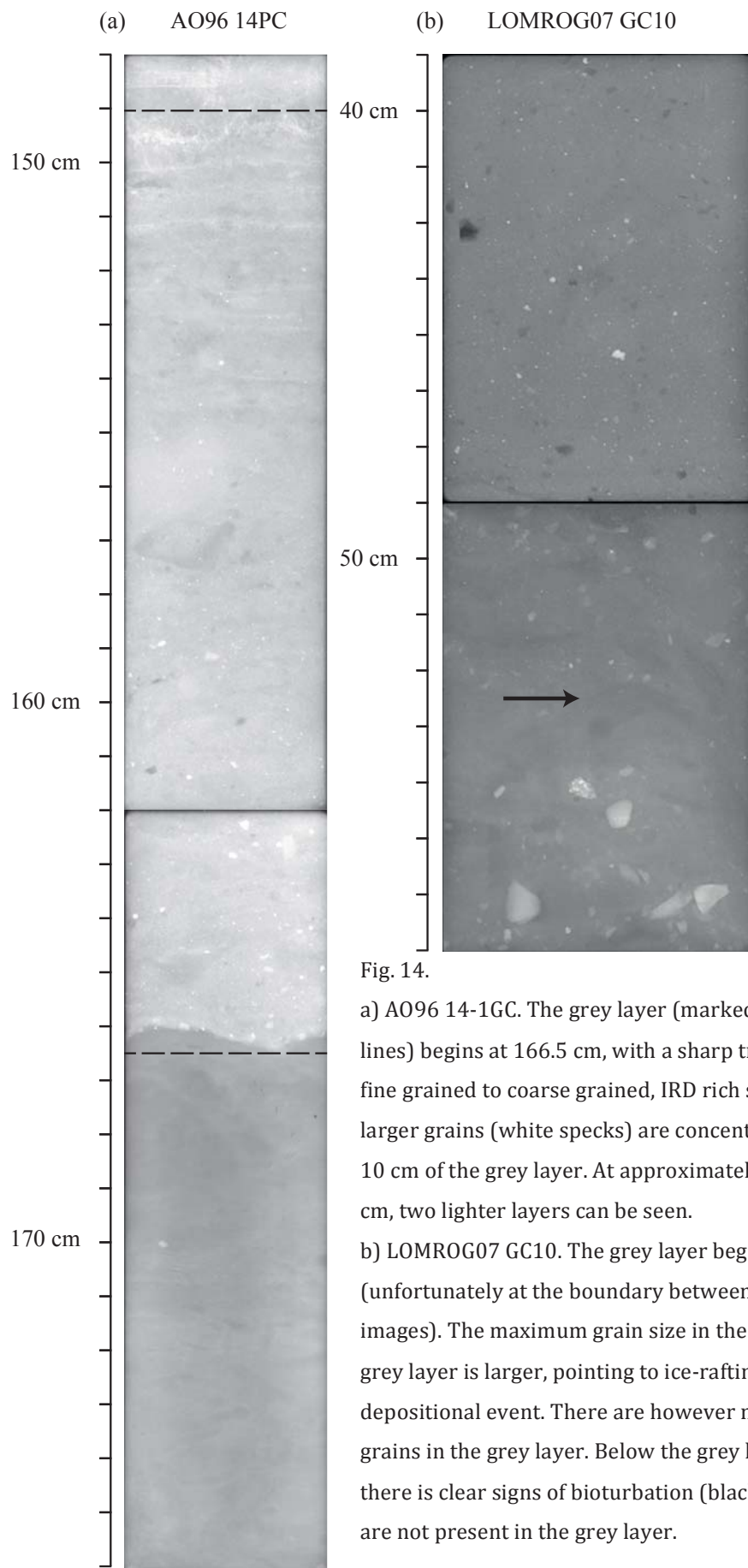


Fig. 14.

a) AO96 14-1GC. The grey layer (marked with dashed lines) begins at 166.5 cm, with a sharp transition from fine grained to coarse grained, IRD rich sediment. Most larger grains (white specks) are concentrated in the first 10 cm of the grey layer. At approximately 151 and 150 cm, two lighter layers can be seen.

b) LOMROG07 GC10. The grey layer begins at 49 cm (unfortunately at the boundary between the two images). The maximum grain size in the 10 cm below the grey layer is larger, pointing to ice-rafting before the depositional event. There are however more coars grains in the grey layer. Below the grey layer boundary, there is clear signs of bioturbation (black arrow), which are not present in the grey layer.

### **6.3 Element concentrations (XRF and TIMS)**

Comparison of Fe and Mn concentrations from XRF scans of cores A096-14-1GC and LOMROG07-GC-10 and concentrations of Sm/Nd from the isotopic analyses show a distinct drop at the transition into the grey layer (Fig. 15). Fe drops by 30% in LOMROG07 GC10 and 50% in A096 14-1GC, while Mn almost completely disappears. Above the grey layer, three Mn peaks could be observed. Mn values are low within and below the grey layer (see Section 3.5). XRF scans of YMER80 132 SGC (Fig. 15) showed little variation in Mn values throughout the core, on average a fifth of the concentrations in LOMROG07-GC10, and a less distinct drop in Fe and Mn values at the beginning of the grey layer. There is a drop in Fe and Mn values at 320 cm core depth, however, based on sedimentation rates of 1-5 cm/ky (Jakobsson et al., 2000; Backman et al., 2004), this is likely too deep in the core to correspond to the 50ka event.

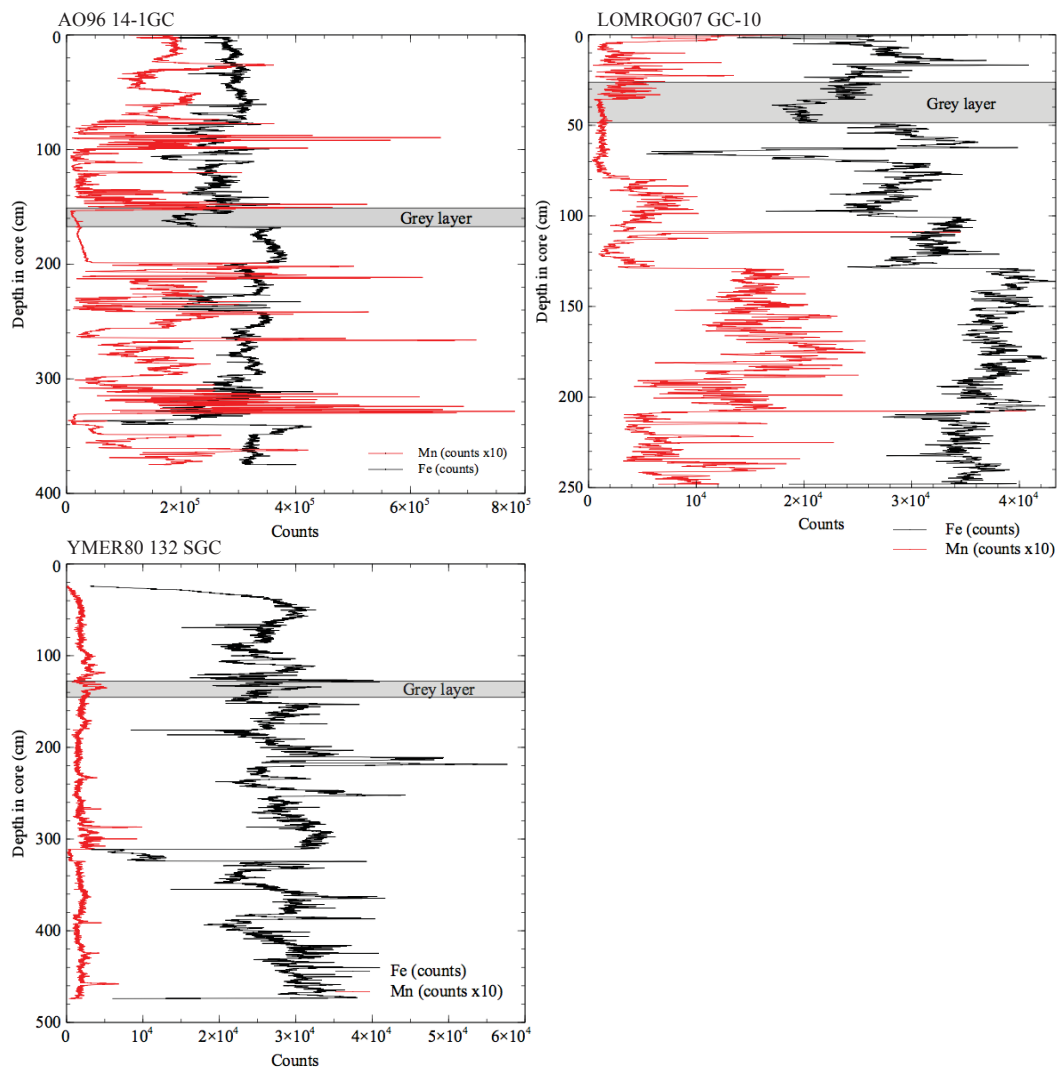


Fig. 15. AO96 14-1GC and LOMROG07 GC-10 show the distinct drop in Fe and Mn. YMER80 132 SGC deviates from this, with no reduction in Fe and Mn at the sampled grey layer. There is a reduction at approximately 320 cm core depth (see section 7.5). Note that the Mn minima continues below the grey layer in core AO96 14-1GC and LOMROG07 GC-10, likely due to a reduction front moving downward in the sediment (see Discussion).

The element analysis by the TIMS showed drops in Nd and Sm concentrations at the lower grey layer boundary (Fig. 16) in cores AO96 14-1GC and LOMROG07 GC10. A drop in Nd was also observed in YMER80 132 SGC, however not at the visual boundary of the sample, but centred in the middle of the grey layer.

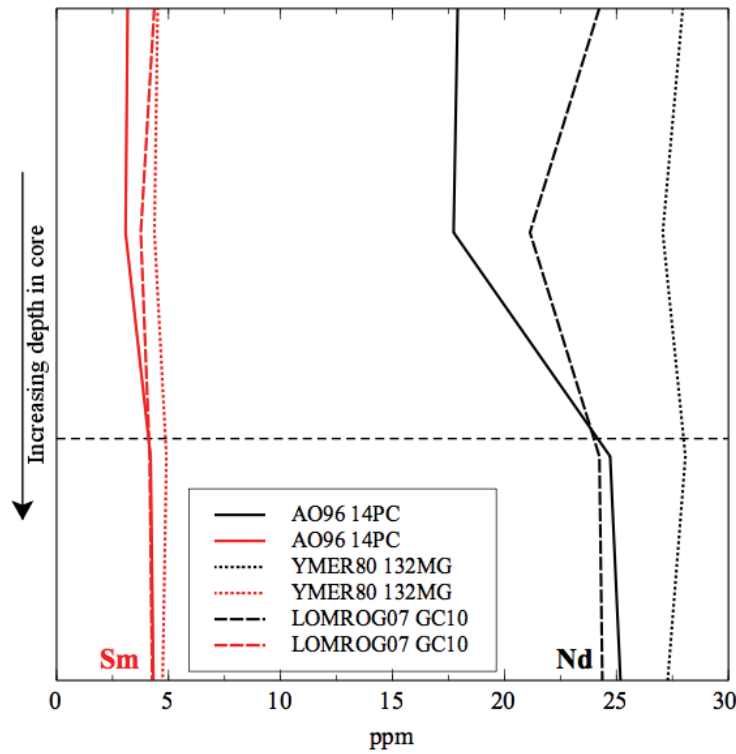


Fig. 16. Concentrations of Nd and Sm in detrital samples from cores AO96 14-1GC, LOMROG07 GC10 and YMER80 132 SGC. Cores AO96 14-1GC and LOMROG07 GC10 show drops of 7 and 3 ppm Nd, respectively, at the transition into the grey layer. Sm decreases by 0.5-1 ppm in the same cores. YMER80 132 SGC only displays smaller decreases in both Nd and Sm.

## 6.4 Radiogenic isotopes

### 6.4.1 Run 1: bulk samples

A trial run of Nd/Sm analysis was conducted on bulk samples from the core A096 14-1GC, at the depths of 140, 150, 160\*, 164\*, 170 and 180 cm from the core top (\*these samples are inside the grey layer). This analysis showed no conclusive difference in Nd or Sm ratios between the grey layer and surrounding sediment (Fig. 17).

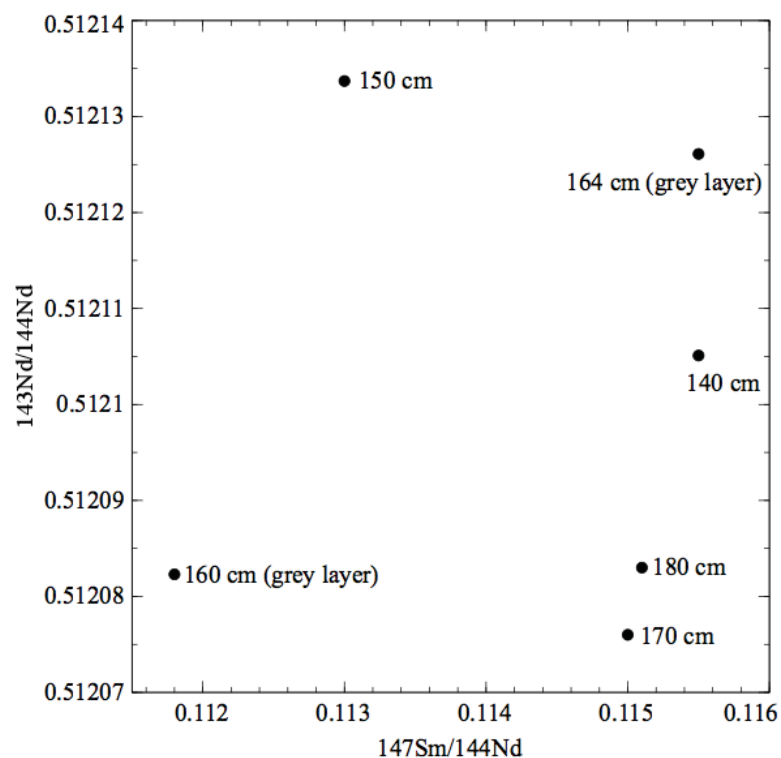


Fig. 17. First bulk run of A096 14-1GC, showing  $^{147}\text{Sm}/^{144}\text{Nd}$  to  $^{143}/^{144}\text{Nd}$  ratios. No conclusive difference was found between the grey layer and surrounding sediment.

### 6.4.2 Run 2: authigenic and detrital material separated

Because the bulk analysis failed to distinguish the grey layer, the samples from A096 14-1GC were run again, however this time the detrital and authigenic fractions were separated (see section 5.2.4). This produced two distinct signals (Fig. 18).

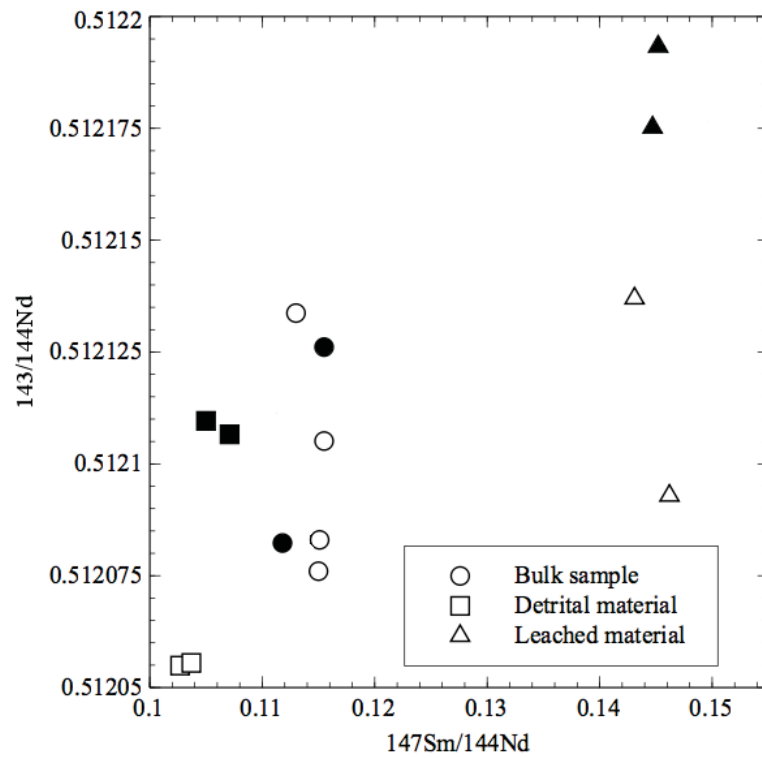


Fig. 18. When separating the leached (triangles) and detrital (squares) fractions, a clear division between grey layer (black fill) and surrounding sediment is visible. Bulk samples (circles) are shown for comparison. Note: error bars are too small to be visible ( $<5.1 \times 10^{-6}$ , or  $<0.001\%$ )

This separation of authigenic material was implemented for all later samples. (Fig. 19). The Putorana plateau isotopic signal shows  $\epsilon\text{Nd}$  values of approximately +3 to -2, with an outlier at -5.68, and  $^{87}/^{86}\text{Sr}$  values ranging from 0.7076 to 0.7040 (Sharma et al., 1992). The transition into the grey layer shows a decrease in  $^{87}/^{86}\text{Sr}$  ratios by approximately 0.05 in all samples, and an increase in  $\epsilon\text{Nd}$  by 1 in core AO96 14-1GC and 2 in YMER80 132 SGC and LOMROG07 GC-10. YMER80 132 SGC however has a higher  $^{87}/^{86}\text{Sr}$  ratio than the other two.

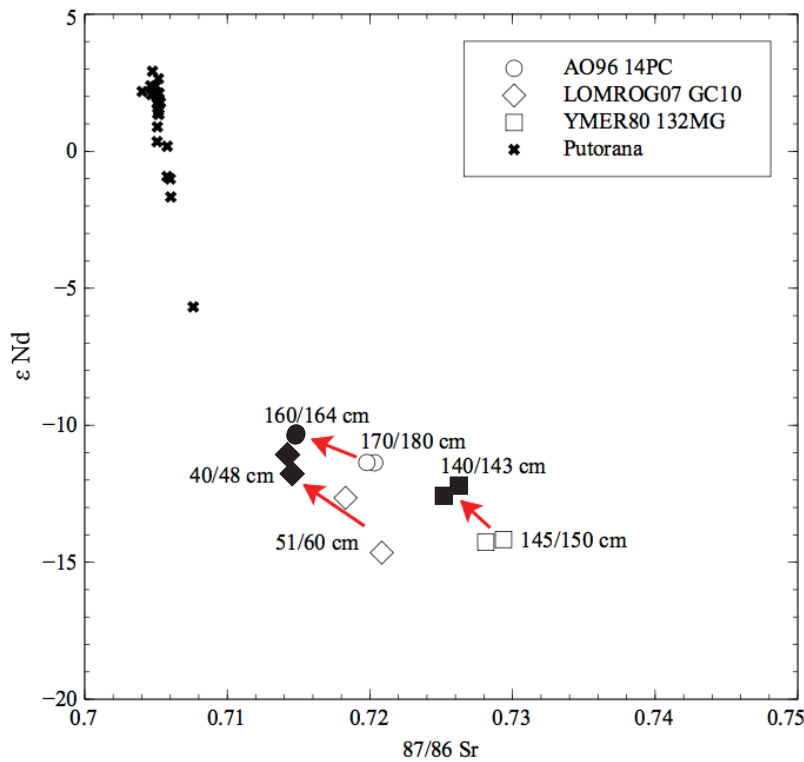


Fig. 19. Comparison of Putorana and detrital samples  $\epsilon\text{Nd}$  vs  $^{87}/^{86}\text{Sr}$ , including detrital from first run. Red arrows show the shift in isotopic values at the transition into the grey layer. Labels denote depth in core. Filled-in data points denote samples in grey layer.

As Fig. 20 shows, cores AO96 14-1GC and LOMROG07 GC10 display an increase in both  $^{147}\text{Sm}/^{144}\text{Nd}$  and  $^{143}/^{144}\text{Nd}$  ratios at the transition into the grey layer. YMER80 132 SGC, however, displays an increase in  $^{143}/^{144}\text{Nd}$ , but a decrease in  $^{147}\text{Sm}/^{144}\text{Nd}$ .

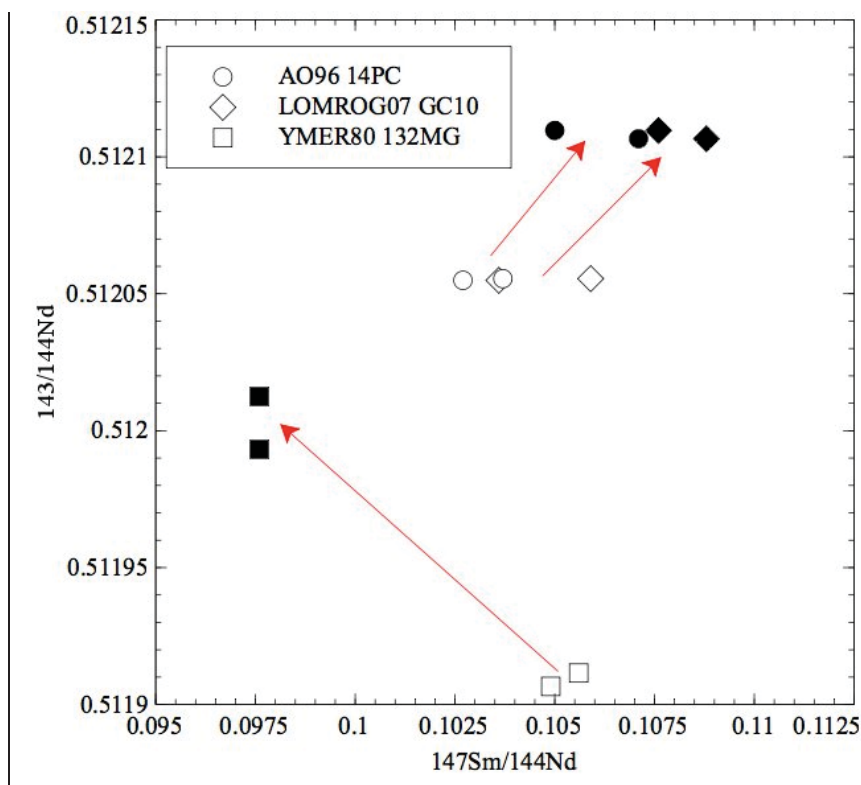


Fig. 20.  $^{147}\text{Sm}/^{144}\text{Nd}$  to  $^{143}/^{144}\text{Nd}$  ratios of samples at the transition into the grey layer. Red arrows mark the change in isotopic composition over the grey layer boundary. Filled-in data points denote samples in grey layer.

## 6.5 Organic carbon

Four cores (AO96 14-1GC, LOMROG07 GC10, YMER80 132 SGC and AO96/B13 1PC) were analysed for total organic matter (TOM) and loss on ignition (LOI). Primary results showed relatively high organic carbon content (3-6 %, Table 2). Twenty-five samples were therefore analysed for  $^{13}/^{12}\text{C}$  and  $^{15}/^{14}\text{N}$ . These analyses, and subsequent reruns with a newly calibrated machine, yielded much lower quantities of organic matter. The large sample weights that would be required to produce reliable  $^{13}/^{12}\text{C}$ - and  $^{15}/^{14}\text{N}$ -results would necessitate too frequent cleaning of the mass spectrometer, leading to high cost and low efficiency. This line of inquiry was therefore discontinued.

Sample number	%wt C <sub>org</sub>	%wt C <sub>org</sub>
14	3.836111669	0.45
15	4.044294656	0.58
16	4.127906977	0.90
17	3.458254956	0.86
18	3.622779814	0.99
19	3.741555517	0.87
20	5.82183187	0.54
21	5.381056732	0.47
22	5.493934142	0.39
23	5.950378469	0.29
24	5.919765166	0.35
25	4.987479132	0.27
26	5.586712683	0.33

Table 2. Comparison of variations in %wt organic carbon between first measurement (3-stage heating to 950 °C and weighing) and second measurement (elemental analyser coupled to isotope ratio mass spectrometer) of samples from core A096 14-1GC

## 7. Discussion

### 7.1 Sediment sources and transport patterns

As the Kara Sea would have been at least partially covered by the Weichselian ice sheet at 60-50 ka, sediment entrained in the ice sheet would contain high amounts of smectite (Wahsner et al., 1999). The ice-dammed lake proposed by Mangerud et al. (2004) covered large parts of the Siberian traps (Fig. 13), and several large rivers drained into it. Weathering products from the Putorana plateau basalt (smectite) transported by these rivers would have been deposited in the lake and entrained in the ice-sheet.

If the grey layer is the product of a catastrophic outburst from an ice-dammed lake near the Putorana plateau, how would this present in the data?

Firstly, we would look at the geographical distribution of the layer. While this outburst would have been a high-energy event, the more coarse-grained sediment would not have been transported far by the flow of water, but rather as IRD in broken-off icebergs from the northern ice sheet margin. An increase in water flow at the base of the ice-sheet can act as a lubricant and increase the

flow rate (Alley et al., 2008), and this could have destabilised the northern edge of the ice-sheet, as calving activity increases when an ice-sheet reaches deeper waters (Siegert et al., 2002). The unstable ice edge would then begin to calve, and large quantities of IRD would be transported into the Arctic Ocean by these icebergs. Compared to conditions before and after the event, there would not be more coarse grained material entrained in the ice; the increase in coarse grained material found in sediments is solely attributed to more ice being dislodged. The material from the outburst would have been directed into the Transpolar Drift, and this current would have swept along most of the dislodged ice, depositing it in the Eurasian Basin, and leaving little trace of the event in the Amerasian Basin. The increase in coarse-grained material left by this would be most prominent at the beginning of the deposited layer, as the finer-grained material takes longer time to settle.

Secondly, the isotopic signature of detrital material in the grey layer would correspond to that of the Putorana plateau, or at least show an increase in material from that area. This increase in Putorana material would have been caused by the ice sheet transporting material from the plateau to the shelf, and the ice-bergs released by the increased calving after the outburst moving the material into the Arctic Ocean.

Thirdly, the drainage could have carried along other material, such as peat and other organic material from the ice-dammed lake and surrounding tundra, and remains of this could be present in the grey layer. Solid organic material could have been transported both as IRD (peat was likely entrained into the ice along with sediment) and by the flow of water. Additionally, humic acids present in the lake would have been carried along, however the concentration of these is difficult to estimate.

## **7.2 Fe and Mn**

As Fe/Mn-oxyhydroxides are redox sensitive (e.g Lewis and Landing, 1991), the rapid decrease in Fe and Mn counts at the grey layer points to suboxic or anoxic conditions, preventing the formation of authigenic minerals, and possibly dissolving much of existing authigenics. A rapid deposition of large amounts of sediment, possibly containing organic material from Siberian peatlands, would

have acted as a lid, preventing the transfer of oxygen from the bottom water to the pore waters.

The redox front created by this would have steadily moved downward, and Fe/Mn-oxyhydroxides dissolved to fuel decomposition of the organic material until no more organic material remained, or until the distance between the organic material and available oxygen was great enough to halt the process. This is consistent with the almost non-existent Mn in and below the grey layer, Mn reacting before Fe (Fig. 10b).

The almost complete dissolution of Mn suggests that it, before the grey layer event, was contained solely within easily dissolved authigenic particles, and not present in the terrigenous material. During the weathering of basalt, Mn is highly mobile, with a 40% (higher during intense weathering) loss of Mn in the source rock (Eggleton et al., 1987). It can therefore be assumed that Mn content in detrital material from the Putorana plateau is relatively low.

Unlike Mn, Fe content is only significantly lowered in the actual grey layer, not below it. If the reducing conditions after the grey layer deposition were responsible for the lower Fe content, we would see the same pattern as with Mn, but we do not. It can therefore be assumed that the cause for Fe change lies not only with authigenics, but also, and possibly primarily, with detrital material. During experiments of basalt weathering, Fe has been shown to be less mobile than Mn (in two experiments, the mass loss of Mn was 40-45 %, while the mass loss of Fe was 0 % [Eggleton et al., 1987]), which would suggest Mn enrichment compared to Fe in solution in water drained from the plateau. Pokrovsky et al. (2005) found consistently higher concentrations of Fe- than Mn-minerals in solid weathering products (soils, suspended matter, river sediments) of the Putorana plateau, suggesting Fe-minerals are more mobile. No Mn-analysis of water was however conducted.

There are several Mn lows, or troughs, in the cores, corresponding with the decreased input of glacial periods and can be tied to colour variations of the sediment (Löwemark et al., 2014). The grey layer is the only extended low in Mn

in A096 14-1GC and LOMROG07 GC-10 (see Fig. 15 and section 7.5 for discussion of YMER80 132 SGC).

### **7.3 Clay mineralogy**

Although no clay mineral analysis was conducted in this study, it has been shown that smectite, a basalt weathering product, is well suited for source area determination of Arctic sediments (Wahsner et al., 1999). High concentrations of smectite are found in the Barents-Kara and Laptev Seas (see section 3.4 and Fig. 6). If an ice sheet was present over these areas, an increase in calving would have led to higher smectite content in sediments later deposited by the melting icebergs. The tripling in smectite content at the transition into the grey layer (Strand and Immonen, 2010) can therefore be explained by increased input of weathering products from the Putorana plateau, i.e. from the Kara or western Laptev Sea.

### **7.4 Nd/Sm analysis**

Initial Nd/Sm analysis gave unclear results; no apparent difference between the grey layer and surrounding sediment was found. As the material in the samples was a mix of detrital and authigenic material, the latter having the same Sm/Nd signature as the sea water (Haley et. al., 2008), running bulk samples gave a mixed signal. However, after separation of authigenic and detrital material was performed, an easily distinguished difference between authigenic and detrital material was observed. Both A096 14-1GC and LOMROG07 GC10 showed similar changes in the isotopic signal of the grey layer; a clear transition toward the Putorana signal. This shift pointed to an increase in the amount of material transported from the Putorana plateau and Putorana-derived sediments. The sediment in the grey layer was clearly not only Putorana-derived, else it would have completely matched the Putorana-signal, but contained material from other sources as well. The shift towards Putorana-like values was of the magnitude 1 (A096 14-1GC) to 3  $\epsilon$ Nd-units (LOMROG07 GC-10) and 0.05  $^{87/86}\text{Sr}$ , with  $2\sigma$  at  $>2.8 \times 10^{-6}$  ( $>0.006\%$  of the change in  $^{87/86}\text{Sr}$ ).

Although the outburst from the ice-dammed lake was great, other water masses must still have been contributing to sediment transport across the Arctic at the time of the event. The TPD, carrying sediment from the Laptev and East Siberia Sea, would dilute the Putorana-signal. Therefore, it is not surprising that the chemical signature of the grey layer does not completely match that of the Putorana plateau. There is also a mixing taking place closer to shore. The Laptev Sea, through which some of the outburst may have passed, has a sediment mix that is 25% Khatanga river (flood basalt) and 75% Lena river (sandstone) derived (Eisenhauer et al., 1999; Dethleff et al., 2000; Viscosi-Shirley et al., 2003).

In order to distinguish what other sources than Putorana-derived sediment constitute the grey layer, according to Tütken (2002) one would have to perform grain size separation.  $^{147}\text{Sm}/^{144}\text{Nd}$  and  $^{87}/^{86}\text{Sr}$  ratios for each grain size would then have to be measured, pinpointing if the source of the other material is constrained to certain grain size intervals. This could then be used to calculate the mixing proportions of the sediment layer. The provenance of larger IRD could also be analysed separately, although this would be even more time consuming. Immonen et al. (2014) used microtextures on IRD, specifically quartz grains, to differentiate between glacial and non-glacial signals in core A096 12-1PC. The microtexture analysis suggests an IRD peak at approximately 60 ka, which could be linked to an ice-dammed lake outburst (Immonen et al., 2014), placing the event earlier than the 50 ka suggested by e.g. Spielhagen et al. (2004).

All cores showed the same pattern of change in Nd and Sm concentrations; a drop at the transition into the grey layer, followed by an increase to normal levels as the layer “faded out”. Nd and Sm adsorbs to, and forms complexes with, Fe/Mn-oxyhydroxides (Tang and Johannesson, 2003). The same anoxic conditions which would dissolve oxyhydroxides and mobilise Fe/Mn would similarly mobilise Nd/Sm. When comparing ITRAX-scans with TIMS-results (Fig. 15 and 16), this indeed seems to be the case, as Nd/Sm show the same pattern in both A096 14-1GC and LOMROG07 GC-10; Nd/Sm follows the fluctuations in Fe/Mn closely. YMER80 132 SGC deviates from this (see section 7.5).

The pH of a solution has been shown to affect adsorption of cations to Mn oxides (Posselt et al., 1968), and the addition of organic matter and humic acids from the peat bogs of Siberia could possibly have affected the pH of Arctic bottom waters; how much is however difficult to determine. A change in pH would have in turn affected the speciation of REEs, as these show an intricate behaviour in a solution where both dissolved organic matter, free cations such as Fe<sup>3+</sup> and Al<sup>3+</sup>, and carbonate ions are present (Tang and Johannesson, 2003).

### 7.5 YMER80 132 SGC – a different grey layer?

Several differences (Table 3) can be found when the grey layer in YMER80 132 SGC is compared to those of AO96 14-1GC and LOMROG07 GC10. <sup>87/86</sup>Sr ratios are higher (Fig. 19), <sup>147</sup>Sm/<sup>144</sup>Nd ratios decrease rather than increase at the grey layer boundary (Fig. 20), element concentrations show a different pattern and ITRAX results are low throughout for Mn (Fig. 15). Tütken (2002) showed that <sup>87/86</sup>Sr ratios are grain size dependent, and this could partly explain the difference between the cores. It does however not explain the different pattern of <sup>147</sup>Sm/<sup>144</sup>Nd change at the grey layer boundary.

Grey layer characteristics in the YMER80 core 132 SGC compared to other cores in study	
Visual	Less distinct lower boundary
IRD	No major difference
XRF (Mn, Fe)	Low Mn throughout YMER80 132 SGC, large variations in AO96 14-1GC and LOMROG07 GC10
Sm/Nd	<sup>147</sup> Sm/ <sup>144</sup> Nd decrease at grey layer boundary, compared to increase in other cores
Sr	Higher <sup>87/86</sup> Sr ratios than in other cores

Table 3. Overview of core YMER80 132 SGC attributes

A possible explanation is a misidentification of the grey layer during visual inspection. The causes for a misidentification can be that the core is old and somewhat dried out, leading to a colour change, or that other events than the 50-60 ka lake outburst could cause grey layers, and without isotope analysis it is difficult to separate them. As YMER80 132 SGC is situated far south, it is possible

that the sediment from the 50-60 ka event did not reach the site, or did so in small enough quantities not to be detected in our analysis. The layer sampled in YMER80 132 SCG could be from a local event, but isotope comparisons to potential sources would be needed to make any conclusions. As with AO96/B13 1PC, which contains four grey layers, earthquakes, common on the nearby Gakkel ridge (Tolstoy et al., 2001), could cause mudslides which may form grey layers.

## **7.6 Difficulties related to grey layer identification**

### 7.6.1 Visual

A grey layer is present in many cores from the Eurasian basin, indicated by visual examination and core descriptions. This method works well for preliminary studies, but has a number of flaws. In the case of core AO96/B13 1PC, four separate grey layers were found, and distinguishing which, if any, of these can be linked to the Weichselian ice-dammed lake in Siberia is impossible without enlisting other methods. Further, older cores such as YMER80 132MG tend to dry out, and this alters their colour and affects grey layer identification.

The 4 grey layers of AO96/B13 1PC can possibly be attributed to local events, e.g. mudslides. Its position on the Gakkel ridge, an active spreading ridge where earthquakes are common (Tolstoy et al., 2001), perhaps makes such a scenario more likely.

### 7.6.2 Radiogenic isotopes

Analysis of Nd, Sm and Sr gave results with high precision for all three cores. Although it requires low amounts of sample (0.10g dried sample for 10-15 runs), it is an expensive and time-consuming method. The results of Sr analysis is also sensitive to grain size variations. For this study it was unfeasible to analyse all grain sizes, as it would fall outside the budget and time constraints, but it would be preferable for a more detailed study. Without radiogenic isotope measurements, it would not have been possible to clearly point out the YMER80

132 SCG grey layer as different from those of A096 14-1GC and LOMROG07 GC10.

## 8. Conclusion

From the isotope analysis of the three cores (AO96 14-1GC, LOMROG07 GC10 and YMER80 132MG), aided by X-ray images and XRF data, the following conclusions can be drawn.

The grey layers found in AO96 14-1GC and LOMROG07 GC10 contain sediments that were likely from the same source; they show almost identical patterns in all analyses. The drop in both Fe and Mn at the grey layer boundary, the low Mn within and below the grey layer, and the three Mn peaks above the grey layer are also indicators that the locations of these two cores were influenced by the same event.

The grey layer in YMER80 132 SCG deviates from these patterns, most noticeably in  $^{87/86}\text{Sr}$  and  $^{147}\text{Sm}/^{144}\text{Nd}$  ratios. A change in grain size could explain the difference in Sr ratios, but not in Sm/Nd. This layer is assumed to have a different origin than those in AO96 14-1GC and LOMROG07 GC10.

Mn was highly affected, Fe less so, by the reducing conditions that would have prevailed after the deposition of the grey layer. The drop in Fe is attributed both to reducing conditions after grey layer deposition, and a different source of detrital material.

Nd and Sm is mobilised when Fe/Mn-oxyhydroxides are dissolved, and the grey layer displays a decrease in the concentration these elements.

The clear shift in  $^{147}\text{Sm}/^{144}\text{Nd}$  to  $^{87/86}\text{Sr}$  towards Putorana-basalt like values in core AO96 14-1GC and LOMROG07 GC10, together with X-ray images, ITRAX scans and smectite content from Löwemark et al. (2009) tie the grey layer to the Putorana plateau, its weathering components and a large outburst that transported this material into the Arctic Ocean.

Based on these findings, the following scenario is proposed:

The outburst from the ice dammed lake, situated west of the Putorana plateau in northern Siberia at about 60-50 ka, initiated the deposition of the grey layer, both via an increase in IRD caused by increased calving and an added flow of finer grained particles, both as IRD and by water-flow. It was a high-energy event that occurred over a short time period, and transported large amounts of sediment into the Arctic Ocean. The drainage time of the Lake Agassiz/Ojibway has been estimated to <100 years (Barber et al., 1999), however this drainage was considerably larger (163000 km<sup>3</sup>, Teller et al., 2002) than that in northern Siberia. The volume of the Siberian lake has been calculated to 32000 km<sup>3</sup> (Mangerud et al., 2004), similar to the 29300 km<sup>3</sup> of the Baltic Ice Lake (Jakobsson et al., 2007). How large the Siberian lake drainage was, is however open to speculation.

The source of the sediment was the Kara Sea or west Laptev Sea, but organic material from the peat bogs, and river sediment that had accumulated in the ice dammed lake was also deposited in the grey layer. Much of this sediment was trapped in icebergs and sea ice, and the abundance of these, containing large-grained material, contributed to the coarser grain size of the grey layer compared to surrounding sediment. The ice carrying sediment would have moved west and south by the force of the outburst and the Transpolar Drift. It appears from core records as though the Yermak Plateau north of Svalbard did not receive much sediment from the event; drainage sediments did however reach as far as the Lomonosov Ridge and the Morris-Jessup Rise.

The breakdown of deposited organic material depleted the oxygen of the pore water in the grey layer and deeper sediment. This caused a reduction front to move downward in the sediments and dissolve Fe and Mn-oxyhydroxides. These diffused toward the sediment surface, and precipitated at the lowermost oxidation front.

Rare earth elements, such as neodymium and samarium, were mobilised, along with the Fe and Mn to which they adsorb, although not to the same extent. The detrital material left by the grey layer, although diluted with sediment from other sources, remained clearly different from surrounding sediment, thanks to

the distinct chemical signature of the Putorana plateau. The outburst left its mark all across the Eurasian basin, where the grey layer is found in over 30 locations.

### **8.1 Future studies**

The number of samples analysed during this study precludes the use of certain statistical tests. Future studies would benefit from a larger sample number, to provide a stronger statistical foundation.

Separation of grain sizes before analysis is preferable in order to avoid uncertainties in Sr measurements.

Source area tracing of larger IRD is another possible avenue of inquiry.

## **9. Acknowledgements**

Ludvig Löwemark, Richard Gyllencreutz and Nina Kirchner for excellent supervision.

Karin Wallner, Per-Olov Persson, Hans Schöberg and Per Andersson at the Laboratory for Isotope Geology, Swedish Museum of Natural History, for invaluable assistance with isotope analyses and for the use of their equipment.

Markus Karasti, Malin Karlén, Francis Freire, Ove Eriksson and Ulla Wennerlund for input and proofreading.

## 10. References

- Backman, J., Jakobsson, M., Løvlie, R., Polyak, L., Febo, L.A., Is the central Arctic Ocean a sediment starved basin?, *Quaternary Science Reviews*, 23, 1435–1454, 2004
- Barber, D. C., Dyke, A., Hillaire-Marcel, C., Jennings, A. E., Andrews, J. T., Kerwin, M. W., Bilodeau, G., McNeely, R., Southon, J., Morehead, M. D., and Gagnon, J.-M., Forcing of the cold event of 8,200 years ago by catastrophic drainage of Laurentide lakes, *Nature*, 400, 22, 1999
- Bjarnadóttir, L.R., Winsborrow, M.C.M., Andreassen, K., Deglaciation of the central Barents Sea, *Quaternary Science Reviews*, 2013 (in press)
- Broecker, W. S., Was the Younger Dryas Triggered by a Flood?, *Science* 312 (5777): 1146–1148, 2006
- Byrne, R., Inorganic speciation of dissolved elements in seawater: the influence of pH on concentration ratios, *Geochem. Trans.*, 3, 2, 11-16, 2002
- DePaolo, D.J. and Wasserburg G.J., Nd isotopic variations and petrogenetic models, *Geophysical Research Letters*, Vol. 3, No. 5, 1976
- Dupré L., Viers J., Dandurand J.-L., Polve M., Bénézeth P., Vervier P., and Braun J.-J., Major and trace elements associated with colloids in organic-rich river waters: Ultrafiltration of natural and spiked solutions., *Chem. Geol.* 160, 63– 80, 1999
- Eggleton, R., Foudoulis, C., and Varkevisser, D., Weathering of basalt: Changes in rock chemistry and mineralogy, *Clays and Clay Minerals*, Vol. 35, No. 3. 161-169, 1987
- Eisenhauer, A., Meyer, H., Rachold, V., Tutken, T., Wiegand, B., Hansen, B.T., Spielhagen, R.F., Lindemann, F., Kassens, H., Grain size separation and sediment mixing in Arctic Ocean sediments: evidence from the strontium isotope systematic, *Chemical Geology*, 158, 173–188, 1999
- Fisher, T.G., Smith, D.G. and Andrews, J.T., Preboreal oscillation caused by a glacial Lake Agassiz flood, *Quaternary Science Reviews*, 21, 873-78, 2002
- Gutjahr, M., Frank M., Stirling, C. H., Klemm, V., van der Flierdt, T., and Halliday, A. N., Reliable extraction of a deepwater trace metal isotope signal from Fe-Mn oxyhydroxide coatings of marine sediments, *Chem. Geol.*, 242, 351– 370, 2007
- Haley, B. A., Frank, M., Spielhagen, R. F., and Fietzke, J., Radiogenic isotope record of Arctic Ocean circulation and weathering inputs of the past 15 million years, *Paleoceanography*, 23, 2008
- Immonen, N., Strand, K., Huusko, A., and Lunkka, J. P., Imprint of late Pleistocene continental processes visible in ice-rafted grains from the central Arctic Ocean, *Quaternary Science Reviews*, in press, 2014
- Ingólfsson Ó. and Landvik, J. Y., The Svalbard-Barents Sea ice-sheet – Historical, current and future perspectives, *Quaternary Science Reviews*, 64, 33-60, 2013
- Jakobsson M., Løvlie R., Al-Hanbali H., Arnold E., Backman J. and Mörth M., Manganese and color cycles in Arctic Ocean sediments constrain Pleistocene chronology, *Geology*, 28, 23–26, 2000
- Jakobsson, M., Grantz, A., Kristoffersen, Y. and Macnab, R., Physiographic provinces of the Arctic Ocean seafloor, *Geological Society of America Bulletin*, 115, 1443-1455, 2003a
- Jakobsson, M., Backman, J., Murray, A., and Løvlie, R., Optically Stimulated Luminescence dating supports central Arctic Ocean cm-scale sedimentation rates, *Geochem. Geophys. Geosyst.*, 4(2), 1016, 2003b.

Jakobsson, M., Björck, S., Alm, G., Andrén, T., Lindeberg, G., Svensson, N.-O., Reconstructing the Younger Dryas ice dammed lake in the Baltic Basin: Bathymetry, area and volume, *Global and Planetary Change*, 57, 355–370, 2007

Jakobsson, M., Backman, J., Rudels, B., Nycander, J., Frank, M., Mayer, L., Jokat, W., Sangiorgi, F., O'Regan, M., Brinkhuis, H., King, J., and Moran, K., The early Miocene onset of a ventilated circulation regime in the Arctic Ocean, *Nature*, 447, 986–990, 2007

Krinner, G., Mangerud, J., Jakobsson, M., Crucifix, M., and Ritz, C., Enhanced ice sheet growth in Eurasia owing to adjacent ice-dammed lakes, *Nature*, 427, 429–432, 2004

Landvik, J.Y., Bondevik, S., Elverhøi, A., Fjeldskaar, W., Mangerud, J., Salvigsen, O., Siegert, M.J., Svendsen, J.I., Vorren, T.O., The last glacial maximum of Svalbard and the Barents Sea Area: ice sheet extent and configuration, *Quaternary Science Reviews*, 17, 43–75, 1998

Lambeck, K., Purcell, A., Funder, S., Kjær, K.H., Larsen, E., and Moller, P., Constraints on the Late Saalian to early Middle Weichselian ice sheet of Eurasia from field data and rebound modeling, *Boreas*, 35, 539–575, 2006

Lee, Sukyoung, A theory for polar amplification from a general circulation perspective, *Asia-Pacific Journal of Atmospheric Sciences*, 50, 1, 31–43, 2014

Löwemark, L., Mellqvist, M., Strand, K., Tessier, H., Jakobsson, M., Evidence for a catastrophic flooding of the Arctic Ocean during MIS 4, *APEX 4<sup>th</sup> Int. Conf.*, Copenhagen, 2009

Murray, J.W., The surface chemistry of hydrous manganese dioxide, *Journal of Colloid and Interface Science*, 46, 3, 357–371, 1974

Murray, J.W., The interaction of metal ions at the manganese dioxide-solution interface, *Geochimica et Cosmochimica Acta*, 39, 606–619, 1975

Michael, P., Thiede, J., Langmuir, C., Jokat, W., Dick, H., Snow, J., Graham, D., Weigelt, E., Goldstein, S., Mühe, R., Edmonds, H., Ritzmann, O., Kurras, G., Büchl, A., Kuhnz, L., Gauger, S., Lehnert, K., Schmidt-Aursch, M. C., Standish, J., Schmidt, T., Broda, J., Schramm, B., Hatzky, J. and Soffer, G., Results of the Arctic Mid-Ocean Ridge Expedition (AMORE 2001) - Seafloor Spreading at the Top of the World, *InterRidge News*, *International Ridge-Crest Research: Arctic Ridges*, 10, 2, 57–60, 2001

Mangerud, J., Jakobsson, M., Alexanderson, H., Ashtakov, V., Clarke, G. K.C., Henriksen, M., Hjort, C., Krinner, G., Lunkka, J.-P., Möller, P., Murray, A., Nikolskaya, O., Saarnisto, M., and Svendsen, J. I., Ice-dammed lakes and rerouting of the drainage of northern Eurasia during the Last Glaciation, *Quaternary Science Reviews*, 23, 1313–1332, 2004

Moran, K., Backman, J., Brinkhuis, H., Clemens, S. C., Cronin, T., Dickens, G. R., Eynaud, F., Gattacceca, J., Jakobsson, M., Jordan, R. W., Kaminski, M., King, J., Koc, N., Krylov, A., Martinez, N., Matthiessen, J., McInroy, D., Moore, T. C., Onodera, J., O'Regan, M., Pälike, H., Rea, B., Rio, D., Sakamoto, T., Smith, D. C., Stein, R., St John, K., Suto, I., Suzuki, N., Takahashi, K., Watanabe, M., Yamamoto, M., Farrell, J., Frank, M., Kubik, P., Jokat, W., and Kristoffersen, Y., The Cenozoic palaeoenvironment of the Arctic Ocean, *Nature*, 441, 2006

Mellqvist, M., New evidence for a mega-event in the Arctic Ocean: Itrax XRF-scanning of cores from the Ymer-80, Arctic Ocean-96 and Lomrog-07 expeditions, Department of Geology and Geochemistry, Stockholm University, 2009

Macdonald, R.W., and Gobeil, C., Manganese Sources and Sinks in the Arctic Ocean with Reference to Periodic Enrichments in Basin Sediments, *Aquat Geochem*, 1–27, 2011

Middag, R., de Baar, H.J.W., Laan, P., Klunder, M.B., Fluvial and hydrothermal input of manganese into the Arctic Ocean *Geochimica et Cosmochimica Acta*, 75, 2393–2408, 2011

Nürnberg, D., Wollenburg, I., Dethleff, D., Eicken, H., Kassens, H., Letzig, T., Reimnitz, E., Thiede, J., Sediments in Arctic sea ice: Implications for entrainment, transport and release, *Marine Geology*, 119, 185-214, 1994

Posselt, H., Anderson, F.J., Weber, W.J. Jr., Cation Sorption on Colloidal Hydrous Manganese Dioxide, *Environ. Sci. Technol.*, 2, 12, 1087–1093, 1968

Palmer, M.R., and Elderfield, H., Rare earth elements and neodymium isotopes in ferromanganese oxide coatings of Cenozoic foraminifera from the Atlantic Ocean\*, *Geochimica et Cosmochimica Acta*, 50, 409-417, 1986

Pokrovsky, O. S., Schott, J., Kudryavtzev, D. I., and Dupré, B., Basalt weathering in Central Siberia under permafrost conditions, *Geochimica et Cosmochimica Acta*, 69, 24, 5659–5680, 2005

Pakhomova, S., and Yakushev, E.V., Manganese and Iron at the Redox Interfaces in the Black Sea, the Baltic Sea, and the Oslo Fjord, *The Handbook of Environmental Chemistry*, Damià Barceló and Andrey G. Kostianoy (eds.), Springer-Verlag Berlin Heidelberg, 2013

Shannon, R.D., Revised Effective Ionic Radii and Systematic Studies of Interatomic Distances in Halides and Chalcogenides, *Acta Cryst.*, 32, 751, 1976

Stein, R., Grobe, H., and Wahsner, M., Organic carbon, carbonate, and clay mineral distributions in eastern central Arctic Ocean surface sediments, *Marine Geology*, 119, 269-285, 1994

Siegert, M. J., Dowdeswell, J. A., Svendsen, J.-I., and Elverhøi, A., The Eurasian Arctic During the Last Ice Age, *American Scientist*, 90, 2002

Spielhagen, R.F., Baumann, K-H., Erlenkeuser, H., Nowaczyk, N.R., Nørgaard-Pedersen, N., Vogt, C., Weiel, D., Arctic Ocean deep-sea record of northern Eurasian ice sheet history, *Quaternary Science Reviews*, 23, 1455–1483, 2004

Stroeve, J., Holland, M. M., Meier, W., Scambos, T., and Serreze, M., Arctic sea ice decline: Faster than forecast, *Geophysical Research Letters*, 34, 2007

Sellén, E., O'Regan, M., Jakobsson, M., Spatial and temporal Arctic Ocean depositional regimes: a key to the evolution of ice drift and current patterns, *Quaternary Science Reviews*, 29, 25–26, 3644–3664, 2010

Strand, K., and Immonen, N., Dynamics of the Barents-Kara ice sheet as revealed by quartz sand grain microtextures of the late Pleistocene Arctic Ocean sediments, *Quaternary Science Reviews*, 29, 2010

Tanizaki Y., Shimokawa T., and Nakamura M., Physicochemical speciation of trace elements in river waters by size fractionation, *Environ. Sci. Tech.*, 26, 1433–1444, 1992

Tütken, T., Eisenhauer A., Wiegand, B., Hansen, B. T., Glacial-interglacial cycles in Sr and Nd isotopic composition of Arctic marine sediments triggered by the Svalbard/Barents Sea ice sheet, *Marine Geology*, 182, 351-372, 2002

Tang, J., and Johannesson, K.H., Speciation of rare earth elements in natural terrestrial waters: Assessing the role of dissolved organic matter from the modeling approach, *Geochimica et Cosmochimica Acta*, 67, 13, 2321–2339, 2003

Wheeler, P. A., Watkins, J. M., and Hansing, R. L., Nutrients, organic carbon and organic nitrogen in the upper water column of the Arctic Ocean: implications for the sources of dissolved organic carbon, *Deep-Sea Research* 11, 44, 8, 1571-1592, 1997

Wahsner, M., Müller, C., Stein, R., Ivanov, G. I., Levitan, M.A., Shelekhova, E.S., Tarasov, G.A., Clay-mineral distribution in surface sediments of the Eurasian Arctic Ocean and continental margin as indicator for source areas and transport pathways - a synthesis, *Boreas*, 28, 1, 215-233, 1999

Li, Y-H., Bischoff, J., Mathieu, G., The migration of manganese in the Arctic basin sediment, *Earth and Planetary Science Letters*, 7, 265-270, 1969

Yakushev, E.V., and Newton, A., Introduction: Redox Interfaces in Marine Waters, *The Handbook of Environmental Chemistry*, Damià Barceló and Andrey G. Kostianoy (eds.), Springer-Verlag Berlin Heidelberg 2013

Zimmermann, B.E., Porcelli, D., Frank, M., Andersson, P.S., Baskaran, M., Lee, D., and Halliday, A.N., Hafnium isotopes in Arctic Ocean water. *Geochim. Cosmochim. Acta.*, 2009

## Appendix 1. Ion exchange, detailed description

### 1a – Elimination of Fe using TRU-spec

1. Biospin column 1 (long adapter), wash with 2 ml **6M HCl** suprapur
2. Biospin column 2 (main, short adapter, tip), add UP-water
3. Col 2: Add prewashed TRU-spec, leave to sediment to 0.5 ml marker
4. Col 2: Wash with 2ml 6M HCl suprapur
5. Place col 1 in col 2, wash with 2 ml 6M suprapur
6. Wash with 2 ml **FC31** (0.3M HF – 0.1M HCl)
7. Condition columns with 2 ml **6M HCl** Seastar
8. Add 0.4 ml of sample (previously dissolved in 4 ml 6M HCl)
9. Collect the 3.6 ml solution left (0.6+1+1+1) in 7 ml Savillex container
10. Wash and collect with 0.5 ml **4M** HCl Seastar via sample container
11. Wash and collect with 0.5 ml 4M HCl Seastar
12. Discard col 1, wash col 2 with 1 ml 4M HCl Seastar to be collected
13. Eluate iron from column using 2 ml FC31
14. To the 5.6 ml Fe-free solution which has been collected, add 1 ml  $\text{HNO}_3$  (conc., Seastar), making it 2.4 M

### 1b – Isolation of REE

1. Condition column 2 using 2 ml 2.4 M  $\text{HNO}_3$  Seastar
2. Heat the eluent (0.05 M  $\text{HNO}_3$ ) in mantled Savillex container to 120 °C
3. Add 0.6 ml of the 2.4 M  $\text{HNO}_3$  sample solution from 1a to the column
4. Add the rest of the sample solution (2+2+2 ml). Collect eluate from p4-7 for Sr analysis
5. Wash and collect via sample container using 0.2 ml 2.4M  $\text{HNO}_3$  Seastar
6. Wash and collect using 0.3 ml 2.4M  $\text{HNO}_3$  Seastar
7. Wash and collect using 0.5 ml 2.4 M  $\text{HNO}_3$  Seastar

8. Wash using 0.2 ml 0.05 M HNO<sub>3</sub> Seastar
9. Mount column over preconditioned LN-spec or collect eluate in this step in 7 ml Savillex container. Eluate REE using 2+1 ml 120 °C 0.05M HNO<sub>3</sub> Seastar

## 2 – Separation of Nd and Sm using LN-spec

1. Remove column from storage. Dry and remove liquid. Purify using 5 ml 1M HCl
2. Condition column using 5 ml 0.16M HCl
3. Add sample from 1b (1+1+1) or mount TRU-spec column from 1b over LN-spec. Make sure it has stopped dripping before p4
4. Wash using 0.2 ml 0.16M HCl
5. Wash using 0.3 ml 0.16M HCl
6. Wash using 0.5 ml 0.16M HCl
7. Wash using 2 ml 0.16M HCl
8. Wash using 1 ml 0.36M HCl
9. Collect Nd in 7 ml Savillex container using 2x2 ml 0.36M HCl
10. Wash using 2 ml 0.36M HCl
11. Prepare for eluation of Sm by adding 0.5 ml 0.6M HCl
12. Collect Sm in 7 ml Savillex container using 3 ml 0.6M HCl
13. Evaporate Nd and Sm to dryness in Al-mount on hotplate at 140 °C. Add a few drops of UP-water and 5 drops conc. HNO<sub>3</sub> and evaporate to dryness. Add H<sub>2</sub>O<sub>2</sub> in turns until sample size no longer is noticeably reduced. Add 1 ml 6M HCl and evaporate to dryness.
14. Purify column using 5 ml 1M HCl
15. Add ca 4 ml 0.25M HCl, let half pass through, then close lid on column and store it.

## 3a – Separation of Sr from matrix

1. Use TRU-spec column from 1a or make new one
2. Heat the eluent (0.05M HNO<sub>3</sub>) in mantled Savillex container to 120 °C

3. Add UP-water to column, make sure there is a flow, then add 120 mg (dry-weight) Sr-spec to 0.5 ml mark (1 mm thick layer)
4. Add pre-washed TRU-spec and leave to sediment to marker ring on column. Mix Sr- and TRU-spec using UP-water. Leave to re-sediment
5. Wash using 2 ml 6M HCl suprapur
6. Wash using 2 ml FC31 (0.3M HF – 0.1M HCl). Repeat p5-6 twice
7. Condition column using 2 ml 2M HNO<sub>3</sub> Seastar
8. Add the 7 ml sample solution collected during 1b
9. Wash using 0.2 ml 2M HNO<sub>3</sub> Seastar
10. Wash using 0.3 ml 2M HNO<sub>3</sub> Seastar
11. Wash using 0.5 ml 2M HNO<sub>3</sub> Seastar
12. Eluate Sr using 2 ml 120 °C 0.05M HNO<sub>3</sub> Seastar into 7 ml Savillex container
13. To collected eluate, add 0.75 ml 8M HNO<sub>3</sub> Seastar and 0.25 ml UP-water, producing a 2M sample-acid-solution

### 3b – Separation of Sr and Ba

1. Reuse column from 3a. Add UP-water to control flow
2. Heat eluent (0.05M HNO<sub>3</sub>) in mantled Savillex container to 120 °C
3. Wash column using 2 ml FC31 (0.3M HF – 0.1M HCl)
4. Condition column using 2 ml 2M HNO<sub>3</sub> Seastar
5. Add the 2M sample-acid-solution to column (2+1 ml)
6. Wash using 0.2 ml 2M HNO<sub>3</sub> Seastar via sample container
7. Wash using 0.3 ml 2M HNO<sub>3</sub> Seastar
8. Wash using 0.5 ml 2M HNO<sub>3</sub> Seastar
9. Wash out barium using 3 ml (2+1) 8M HNO<sub>3</sub> Seastar
10. Prepare for eluation by adding 0.5 ml 2M HNO<sub>3</sub> Seastar
11. Eluate Sr using 2 ml 120 °C 0.05M HNO<sub>3</sub> Seastar into 7 ml Savillex container
12. Evaporate to dryness in Al-mount on hotplate at 140 °C. Add a few drops of UP-water and 5 drops conc. HNO<sub>3</sub> and evaporate to dryness. The following may affect analysis, and was not used in

this study, but is optional: Add H<sub>2</sub>O<sub>2</sub> in turns until sample size no longer is noticeably reduced.

## Appendix 2. Mass spectrometry

The mass spectrometer used was a TRITON™ *Plus* multicollector thermal ionization mass spectrometer (TIMS), located at the Swedish Museum of Natural History.

Nd/Sm samples were analysed on a Thermo Scientific TRITON TIMS using total spiking with a mixed <sup>147</sup>Sm/<sup>150</sup>Nd spike. Concentrations and ratios were reduced assuming exponential fractionation. Samarium concentrations were determined in multicollector static mode on rhenium double filaments. Samarium ratios were normalised to <sup>149</sup>Sm/<sup>148</sup>Sm = 1.22937. Neodymium was run in static mode on double rhenium filaments using rotating gain compensation. Calculated ratios were normalised to <sup>146</sup>Nd/<sup>144</sup>Nd = 0.7219. The external precision for <sup>143</sup>Nd/<sup>144</sup>Nd as judged from values for La Jolla standard ref was 9.0 ppm. Accuracy correction was not necessary since the mean <sup>143</sup>Nd/<sup>144</sup>Nd ratio was 0.5118484±46 (n=32). 2σ error for <sup>143</sup>Nd/<sup>144</sup>Nd was <0.0000081. Depleted mantle age calculated according to DePaolo (1981).

The Sr samples were analysed on a Thermo Scientific TRITON TIMS using a load of purified sample mixed with tantalum activator on a single rhenium filament. Two hundred 8 sec. integrations were recorded in multicollector static mode, applying rotating gain compensation. Measured <sup>87</sup>Sr intensities were corrected for Rb interference using <sup>87</sup>Rb/<sup>85</sup>Rb = 0.38600 and ratios were reduced using the exponential fractionation law and <sup>88</sup>Sr/<sup>86</sup>Sr = 8.375209. The external precision for <sup>87</sup>Sr/<sup>86</sup>Sr as judged from running 987 standard was 8 ppm (n=12), while repeated measurements of prepared CIT #39 sea water gave a reproducibility of ±0.0000083 or 12 ppm (n=14) which is taken to be the best estimate of the external precision. An accuracy correction has to be done, while the <sup>87</sup>Sr/<sup>86</sup>Sr ratio for the NBS 987 standard was 0.710217±06 (n=12). 2σ error for <sup>87</sup>/<sup>86</sup>Sr <0.0000089.